Evaluation of the Thermo-Osmotic Energy Conversion (TOEC) Process for Harvesting Low-Grade Heat Energy

by

Kazem Moradi

A thesis submitted in partial fulfillment of the requirements for the degree of

Master of Science

Department of Mechanical Engineering
University of Alberta

Abstract

The growing global demand for energy, coupled with the need for sustainable and efficient energy solutions, has driven the exploration of new energy sources. Low-grade heat, widely available but challenging to convert into usable forms of energy (such as electricity), is a focal point for addressing this energy dilemma. Thermo-osmotic energy conversion (TOEC) has emerged as a promising technology that harnesses electrical energy from low-grade heat sources. This process relies on a hydrophobic membrane to facilitate the transfer of water vapor molecules from a moderately hot aqueous solution to a colder water stream, creating hydraulic pressure that can be harnessed for electricity generation through a hydro-turbine.

This thesis comprises three comprehensive chapters, each contributing to the understanding and advancement of TOEC technology. The first chapter underscores the significance of harvesting low-grade waste heat for energy conversion, emphasizing the pivotal role of membrane technology in renewable energy solutions. It delves into the challenges and opportunities inherent in the TOEC process, emphasizing the necessity for advancements in utilizing low-grade heat for sustainable energy solutions in the 21st century.

The second chapter delves into the development of a comprehensive model for simulating heat and mass transfer within the TOEC process. The innovative application of the ε-NTU method and a detailed examination of various input variables expand the analytical toolkit available for understanding TOEC systems. The chapter presents a theoretical evaluation of the TOEC process based on mass and heat transfer phenomena, validated with experimental data. Our results indicate that employing membranes with smaller pore sizes, low thickness and high porosity, feed temperature, and flowrates can significantly enhance energy efficiency and power density.

Specifically, we demonstrate that the utilization of hydrophobic membranes with nanometer-sized pores, coupled with hydraulic pressures ranging from 6.2 bar to 11.8 bar, enables us to achieve power densities exceeding 5 W/m^2, given a 20 °C heat sink and a heat source temperature above 65 °C. Furthermore, we have determined that an applied hydraulic pressure of 9.4 bar yields the maximum energy efficiency value of 0.016%. The model offers insights into optimizing the TOEC process, providing pathways for practical applications.

The third chapter introduces a comprehensive life-cycle assessment of membrane synthesis for the TOEC process, addressing a crucial aspect of TOEC technology: the selection of membrane materials. Polyvinylidene fluoride (PVDF) and polytetrafluoroethylene (PTFE) are commonly used materials. This study presents the first-ever comprehensive life cycle assessment (LCA) of PTFE and PVDF membranes, covering both lab-scale synthesis and large-scale production. The assessment evaluates their environmental impact and cumulative energy demand (CED). In the small-scale assessment, key chemical contributors to the CED and environmental impacts of both membranes were identified. In the large-scale analysis, we aimed to assess PTFE and PVDF membranes for electricity generation. The results demonstrate that the PVDF membrane exhibits higher CED than the PTFE membrane for all energy sources except non-renewable biomass. Furthermore, PVDF membrane tends to exert a greater environmental footprint in most impact categories, apart from global warming and ozone depletion. The results provide crucial insights into the environmental implications of membrane materials, aiding in the selection of materials for TOEC applications and advancing sustainable energy generation.

This thesis not only consolidates the understanding of TOEC technology but also paves the way for continued advancements in the pursuit of efficient and environmentally conscious energy generation, marking a notable step towards a sustainable energy future.

Preface

This thesis is an original work by Kazem Moradi and investigates the performance of the Thermo-Osmotic Energy Conversion (TOEC) process for utilizing low-grade waste heat.

Parts of chapter 1 have been published in the *Chemical Reviews*. Title: "Harvesting Blue Energy Based on Salinity and Temperature Gradient: Challenges, Solutions, and Opportunities".

Chapter 2 of this thesis has been published as "Performance Analysis of the Thermo Osmotic Energy Conversion (TOEC) Process for Harvesting Low-Grade Heat" in the *Chemical Engineering Journal Advances*.

Chapter 3 of this thesis is ready for submission to the *Journal of Membrane Science Letters*. The title is "Life-Cycle Assessment of Membrane Synthesis for the Application of Thermo-Osmotic Energy Conversion Process".

Dedicated to

My lovely parents

For their sacrifices and support

Acknowledgments

Table of Contents

List of Tables

List of Figures

Abbreviations

CED	Cumulative energy demand
COF	Covalent organic framework
CNTs	Carbon nanotubes
CTS	Chitosan
CTUe	Comparative Toxic Unit for Ecosystem
CTUh	Comparative Toxic Unit for Humans
DCMD	Direct contact membrane distillation
DI	Deionized
TRECs	Thermally regenerative electrochemical cycles
TOEC	Thermo-osmotic energy conversion
ε-NTU	Effectiveness number of transfer units
FAS	Fluoroalkyl silane
LCA	Life cycle assessment
LCIA	Life cycle impact assessment
LCI	Life cycle inventory
LEP	Liquid entry pressure
MOFs	Metal oxide frameworks
OM	Omniphobic
PDA	Polydopamine
PFO	Perfluorooctanoate
PRO	Pressure retarded osmosis
PRMD	Pressure retarded membrane distillation
PTFE	Polytetrafluoroethylene
PVDF	Polyvinylidene difluoride
SH	Superhydrophobic
SiNP	Silica nanoparticle
SNCs	Silica nanochannels
TECs	Thermo-electrochemical cells
TP	Temperature polarization
WCA	Water contact angle

1   Introduction

1.1. Background and overview of the TOEC process

More than 90% of global energy is consumed or wasted thermally [1]. However, most of the global energy storage capacity has been based on electrochemical systems. Therefore, improving thermal energy storage systems is critical to sustainable development in the twenty-first century. Each year, the volume of industrial waste heat is recorded to be over 8000 TWh per annum in the United States alone [2]. In 2007, 92.4% of the global waste heat from power plants was below 150 °C, classifying them as a low-grade heat resource [3]. Transforming low-grade waste heat into electric power is considered an attractive approach for harvesting renewable energy sources. Liquid-based technologies, including thermo-electrochemical cells (TECs), thermo-osmotic energy conversion (TOEC) systems, and thermally regenerative electrochemical cycles (TRECs), utilize low-grade heat resources to generate electricity [4–6]. The basis of the TOEC technology is the traditional direct contact membrane distillation (DCMD) process, in which a temperature gradient drives vapor migration through a microporous hydrophobic membrane from a warm reservoir to a cold one. This leads to an osmotic pressure difference in the system, as represented in **Figure 1.1.** [7,8]. Like the pressure retarded osmosis (PRO) process, accumulated water in the cold chamber can be depressurized through an inline hydro turbine. Hence, some researchers refer to TOEC as "pressure retarded membrane distillation (PRMD)" [9]. The performance of the TOEC process relies on the characteristics of the utilized porous membrane that allows the operating fluid to flow only in its gaseous state, and the fluid does not wet it. Owing to the temperature difference across the membrane, relative vapor pressure on the hot side will increase, which causes a net vapor flux from the hot to the cold side of the membrane. Utilizing low-temperature heat sources, a vapor flow is passed across the hydrophobic membrane while hydraulic pressure is applied, which provides power densities comparable to other membrane-based power generation methods [10].

1
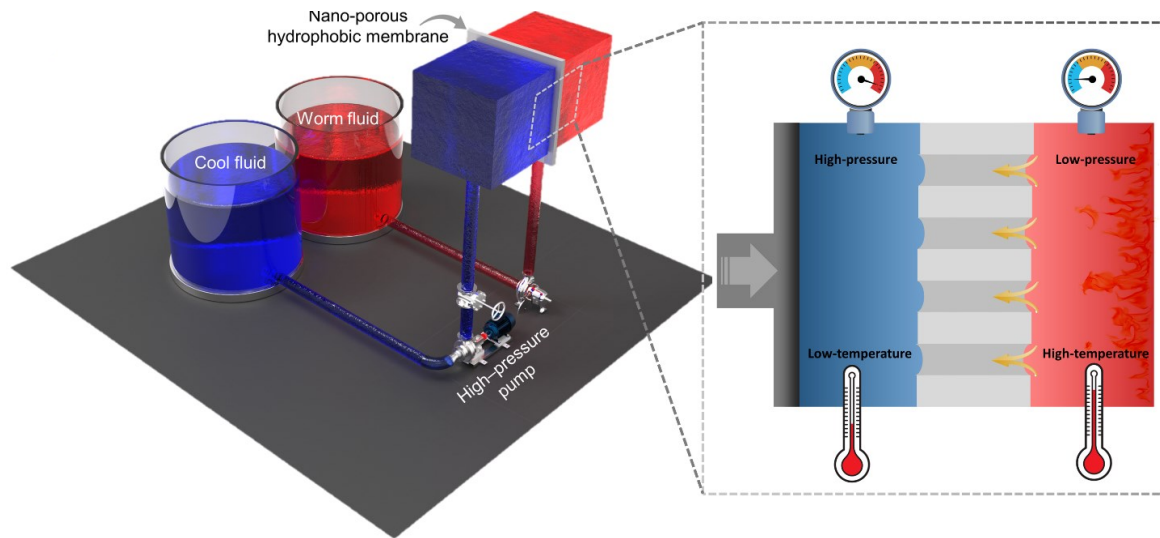
Figure 1.1. Working principle of the TOEC process [11].

1.2. Literature review

1.2.1. Challenges of the large-scale development of TOEC

As explained previously, TOEC has been identified as a promising technology for energy harvesting from low-grade heat resources. However, this technology is in the very early stages of progress, and still, many steps are left for its full-scale commercialization. Essential performance measurement metrics, such as the required power output for real-world viability, membrane specifications, and energy conversion performance, have not yet been developed for a large-scale plant. Only a few studies have been conducted so far on a lab scale. The specific challenges, potential solution strategies, and possible development opportunities need to be precisely evaluated in the case of TOEC. To realize the economic viability and potential opportunity for this technology, accurate determination of metrics and challenges that hinder the application of the TOEC process is crucial. In this regard, power density and heat-to-electricity energy conversion efficiency are two critical metrics for the performance evaluation of the TOEC system. Due to the operational similarity, some TOEC challenges and corresponding solutions will be discussed based on the information and scientific knowledge investigated for the DCMD process.

1.2.1.1. Membrane deformation under applied pressure

Studying TOEC membrane deformation and change of other properties with mass and heat transfer under hydraulic pressure is vital for upscaling this technology. Heat and mass transfer rates through the membrane are highly dependent on the thickness of the membrane. While thinner membranes possess a lower vapor transport resistance, they provide a higher heat transfer rate across the membrane, resulting in very low energy conversion efficiencies. However, high power densities can be obtained with lower membrane thicknesses due to the increased vapor permeability [10]. Such a trade-off is displayed in **Figure 1.2.A**, where both high energy conversion efficiency and power density can be achieved with membrane thickness in the range of 30–100 μm [10]. However, such thin membranes will likely deform under the applied hydraulic pressure [12].

1.2.1.2. Temperature polarization (TP)

Due to the imperfect thermal insulation of the membranes, the actual temperature gradient at the water-membrane interface is lower than the bulk solutions' temperature difference (**Figure 1.2.B**). This phenomenon occurs through the heat transfer from the hot side to the cold side, creating thermal boundary layers on either side of a membrane, which results in a lower vapor flux [13]. The distillate flux rate and energy efficiency are negatively impacted by the TP [14]. In some extreme cases, TP can drop the initial water vapor passage over 50-80%, demanding extensive energy input to keep stable water flux along with the membrane module [15]. The heat transfer coefficient can be analyzed to determine the intensity of temperature polarization. Enhancing the hydrodynamic mixing at the surface can be achieved by increasing cross-flow velocity or using spacers to trigger turbulence in the channel, leading to a higher heat transfer coefficient or reduced temperature polarization [16]. However, the balance between the energy costs of pumping and enhancing both power density and energy efficiency should be considered for selecting an effective heat transfer coefficient. Membrane thermal conductivity is another vital property that must be minimized. Since air is a better insulator than polymers or other materials used in membrane fabrication, developing membranes with higher porosity reduces membrane thermal conductivity [17]. Increasing membrane porosity for TOEC applications requires caution to maintain mechanical robustness and sustained operation under high pressures. Furthermore, reductions in thermal conductivity are feasible using more insulating membrane materials. **Figure 1.2.C** shows the impact of membrane thermal conductivity on energy conversion efficiency and power density.

1.2.1.3. Pore wetting and membrane fouling

The application of traditional hydrophobic membranes in TOEC is limited primarily due to the wetting and fouling of these membranes. The presence of surfactants and oils in aqueous feed streams decreases the surface tension of these media, and the attachment of these contaminants to hydrophobic membrane surfaces results in membrane fouling and pore wetting [18]. Surfactants that are commonly used as the basic constituents of a variety of products such as detergents, paints, cosmetics, pharmaceuticals, pesticides, fibers, and plastics are amphiphilic compounds made up of lyophilic head groups (affinity for polar media) and lyophobic tails (affinity for non-polar media) [19]. The hydrophobic tails attached to the hydrophobic membrane pore surface expose the hydrophilic head, and thus, they result in the hydrophilic pores [20]. Low surface tension contaminants (e.g., alcohol) and surfactants can adsorb onto surfaces and considerably decrease the medium's surface- or interfacial tension [21]. Oils, however, are hydrophobic pollutants with low surface tension. Because of the continuous growth of oil-related sectors, they are discharged into the environment on a massive scale [21]. The primary mechanism of oil fouling is its long-ranged, hydrophobic interactions [22]. Biological microorganisms in water can also promote biofilm growth over the MD membranes [23]. Minerals in the water can cause scaling over the membrane surface due to the high temperature of the hot stream. Both fouling and scaling reduce the membrane permeability coefficient while increasing the thermal conduction coefficient [24].

1.2.1.4. Low liquid entry pressure (LEP)

Figure 1.2.D displays the relationship between energy conversion efficiency and the hydraulic pressure difference across the membrane in the TOEC system. Different lines correspond to the membranes with different surface areas. The optimal energy conversion efficiency can be attained when a reasonable amount of hydraulic pressure is applied over the TOEC membrane. Applying pressure below a certain level decreases the harvested energy sharply and causes process failure [25]. The traditional hydrophobic membranes used in DCMD suffer from low LEP, which is the pressure at which liquid can overcome hydrophobic forces and permeate through the membrane pores in liquid form [26]. Membrane pore size, the surface energy of membrane material (which regulates membrane hydrophobicity), the surface tension of the solution, feed concentration, and the presence of organic solutes are key factors influencing LEP [15,27]. For the real-world application of TOEC, it is essential to design a system with higher LEP that can operate under

higher pressures and, thus, increase the amount of energy harvested by the system. A high LEP can be obtained in membranes with a high contact angle (high hydrophobicity), small pore size, low surface energy, and high surface tension for the feed solution [27,28].
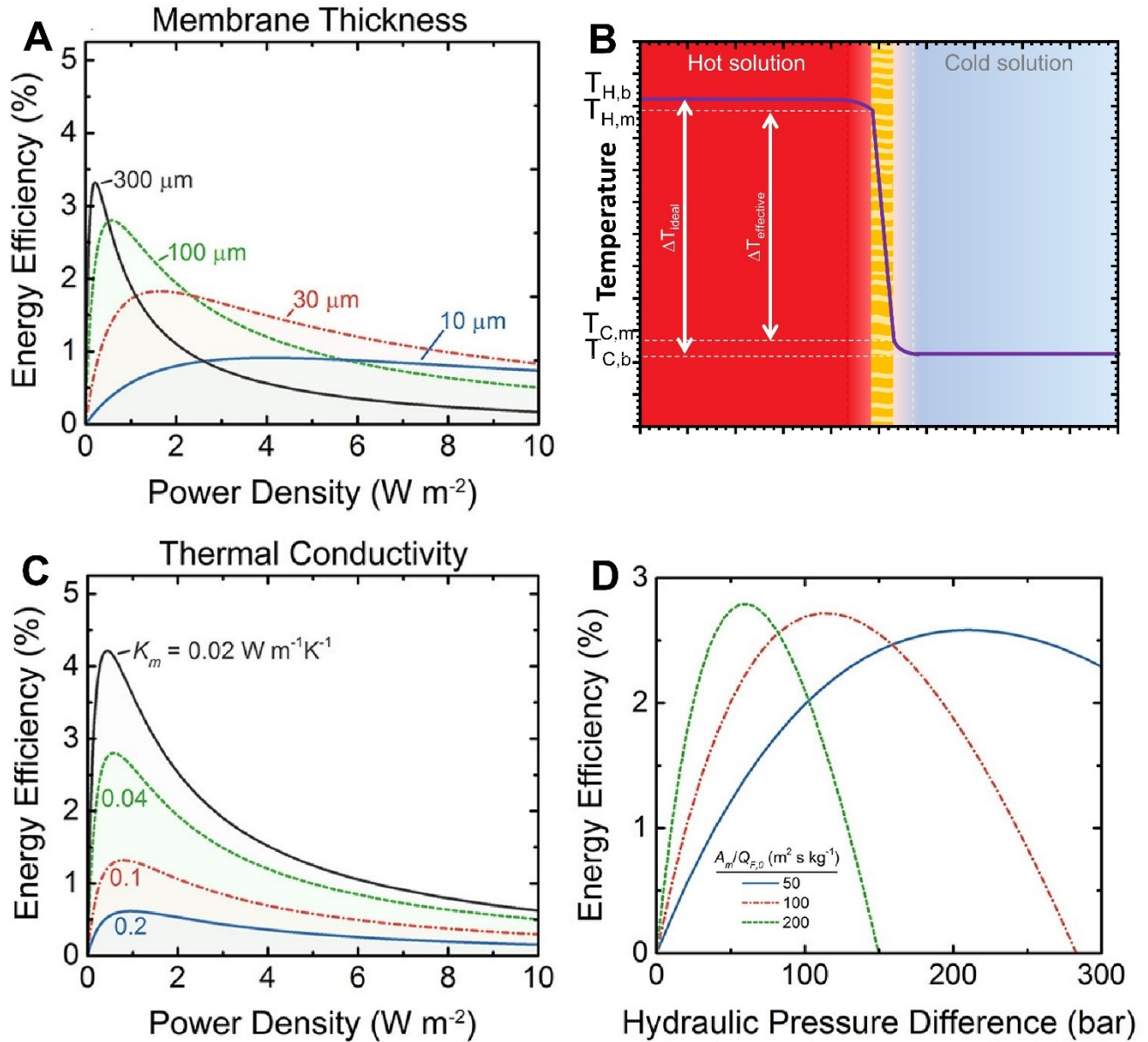
Figure 1.2. (A) The influence of membrane thickness on energy efficiency and power density in the TOEC process, (B) TP profile around TOEC membrane, (C) membrane thermal conductivity impact on the generated power density and energy efficiency of TOEC process, and (D) Energy conversion efficiency as a function of the hydraulic pressure difference across the membrane for TOEC systems. Figures A, C, and D are adapted with permission from REF [10].

1.2.2. Solutions and opportunities for the development of TOEC

The previous section identified various major limitations of the TOEC system for harvesting low-grade waste heat. This section presents some potential responses discussed in the literature that may assist researchers in successfully implementing this system on a large scale.

1.2.2.1. Membrane surface modifications

(i) Superhydrophobic (SH) membranes

The research studies conducted on the MD process show that fouling/scaling fails to meet the same performance as conventional hydrophobic membranes with a water contact angle (WCA) above 90° [29]. Superhydrophobic membranes have WCA above 150° with a contact angle hysteresis (the difference between advancing and receding contact angles) less than 5° [30]. Two major techniques have been proposed so far to induce superhydrophobic surface properties: morphological templating and chemical modifications. The former includes mimicking the surface pattern of lotus leaves to promote SH properties by increasing the surface tension of water. For instance, a hierarchically structured SH membrane was fabricated through the electrospinning technique, which showed a superior water flux of 38 ± 2 LMH and salt rejection of 99.9% under a temperature difference of 40 °C for a 200 h operation time [31]. In another study, Zhao et al. developed and manufactured a hierarchically textured superhydrophobic PVDF membrane using the nanocasting technique [32]. In this technique, two hierarchically textured PVDF membranes with different surface patterns were prepared using a stainless-steel mesh and PDMS template support during the membrane casting. In the second approach, MD membranes were made by roughening hydrophobic surfaces with inorganic nanoparticles (e.g., titanium oxide) [33,34] or microparticle coatings [35]. A tri-bore PVDF hollow fiber membrane with superhydrophobic Teflon AF2400 coating revealed improved anti-wetting characteristics (LEP increased by 109 %). The average water flux and salt rejection reached 21 LMH and 99.99%, respectively, in long-term DCMD operations with synthetic feedwater [36]. The superior anti-wetting properties of coated membranes can be attributed to their lower surface tension, smaller pore size, and low surface energy.

(ii) Omniphobic (OM) membranes

Omniphobic membranes are resistant to wetting by water and low-surface-tension liquids (such as oil), as well as feed solutions containing surfactants that are prevented from entering the membrane pores [37–40]. The key to achieving omniphobicity is incorporating single/multi-level re-entrant structures to the membrane surface and attaining low surface energy [40–42]. Oil droplets cannot permeate through the OM membranes due to the reentrant structure, distinguishing them from hydrophobic membranes [20]. In a reentrant structure, the porous solid surface and the trapped air inside of it can make the entrance of low-surface-tension liquids into the pores energetically unfavorable. Embedding nanoparticle clusters within the porous structure of membranes can also improve the impact of the reentrant mechanism, where the membrane resistance against pore wetting by oil will be favorably increased. To fabricate OM membranes, SiNPs were coated on MD membranes to obtain single/multi-level re-entrant structures on the membrane surface, and the fibrous substrate was functionalized with fluoroalkyl silane (FAS) to reduce membrane surface energy [43,44]. In another study, surface fluorination and polymer coating were carried out on a hydrophilic glass fiber membrane with silica nanoparticles [45]. The fabricated OM membrane sustained a robust DCMD operation with a feed solution containing surfactants. This membrane could provide 9 h constant water permeation with almost 100% salt rejection.

(iii) Janus membrane composed of a hydrophobic substrate with a hydrophilic skin layer

Recent studies have shown that an in-air hydrophilic (or underwater oleophobic) coating over hydrophobic membranes may prevent non-polar pollutants from attaching to the membrane [46,47]. These membranes have shown strong resistance to oil fouling due to the formation of a hydration shell on the hydrophilic coating, which makes them superoleophobic underwater. Lin et al. fabricated superhydrophilic membranes with an in-air contact angle of $15 \pm 1.3°$ by spray coating a perfluorooctanoate/chitosan/silica nanoparticle (PFO/CTS/SiNP) nanoparticle-polymer composite onto a PVDF membrane [20]. Recently, Chew et al. co-immobilized silver nanoparticles with polydopamine (PDA) on a commercial hollow fiber PVDF membrane for MD applications [48]. This membrane showed self-healing and antibacterial properties, and the surface hydrophilicity improved up to 88% compared to the pristine PVDF membrane. In another study, Chen et al. grafted a thin layer of PDA-PEI over the PVDF flat sheet membrane to reduce fouling in the DCMD process [49]. Chen et al. also coated cationic PEI and anionic poly(sodium 4-styrene

sulfonate) (PSS) polyelectrolytes through layer-by-layer assembly on a hydrophobic PVDF membrane [50]. A membrane with three bilayers of PEI/PSS coating demonstrated 36 h water permeation with no failure in salt rejection in the presence of 0.4 nM SDS surfactant. Feng et al. fabricated a Janus membrane by modifying the surface PVDF support using PVA [51]. With 0.05 mM SDS in the feed water, the PVA-modified membrane maintained 100% salt rejection for over 9 h. The wetting resistance of the PVA-modified membrane was compared with the pristine PVDF membrane via ethanol−water mixture breakthrough pressure experiments. As displayed in **Figure 1.3.A**, the PVDF membrane had a breakthrough pressure of 2.7 ± 0.2 kPa, which was increased to 570.0 ± 10.0 kPa in the case of PVA/PVDF membrane. To explain such a surprisingly high LEP, Feng et al. presented interesting wetting and anti-wetting mechanisms for different membranes, as shown in **Figure 1.3.B**. When the pristine PVDF membrane (left side) comes in contact with the SDS-containing feed solution, its LEP reduces due to lower surface tension. Once the applied hydraulic pressure exceeds the LEP value, the membrane becomes readily wet. In contrast, the SDS-containing feed solution easily wets PVA/PDVF Janus membrane through strong capillary forces. The extents of such capillary forces are several orders of magnitude higher than the hydraulic pressure. Therefore, a much higher hydraulic pressure must be applied in this case to overcome the water capillary force in the skin PVA layer.
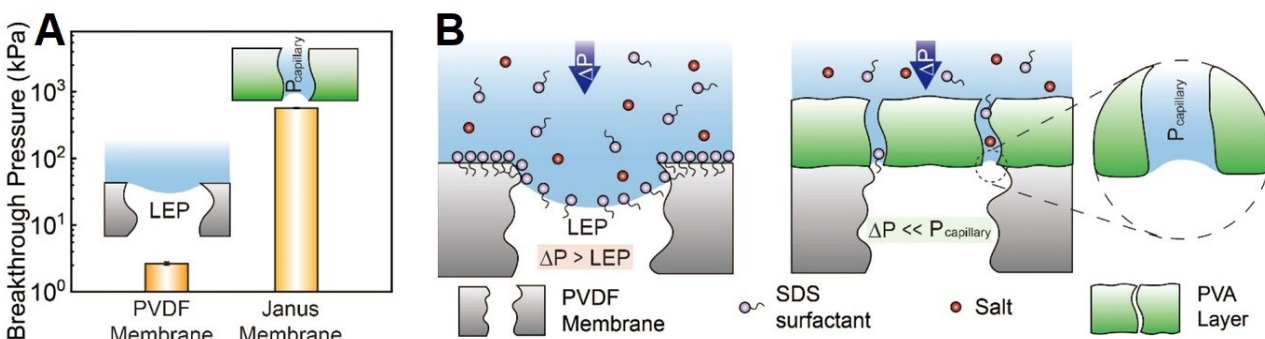
Figure 1.3. (A) Comparison of breakthrough pressures of the pristine PVDF and Janus PVA/PVDF membranes and (B) schematic illustration of wetting and anti-wetting mechanisms proposed for the PVDF and Janus PVA/PVDF membranes. Both figures are adopted with permission from REF [51].

(iv) Ceramic membranes with hydrophobic surface

Ceramic membranes are naturally hydrophilic, but hydrophobic surface modifications can change their water affinity, which makes them suitable for MD and TOEC applications. The main advantage of ceramic membranes is their high thermal and chemical stabilities [52]. Three techniques, including immersion, CVD, and sol-gel, are commonly used for surface modification of ceramic membranes in which hydrophobicity and LEP are mutually improved. Hendren et al. found that hydrophobic alumina ceramic membranes have two times higher LEP values than polymeric membranes [53]. Tested ceramic and polymeric membranes had very similar mean pore diameters and contact angles. However, the large discrepancy in LEP might be attributed to their different pore geometry.

1.2.2.2. Novel membranes

(i) Metallic membranes

Metallic membranes demonstrate excellent mechanical, chemical, and thermal properties, while low distillate flux challenges their incorporation in MD and TOEC processes. These membranes have a high thermal conductivity, which leads to extensive heat loss through the membrane and lowers the apparent distillate flux. However, their natural electrical conductivity indicates another opportunity for "Joule heating" to increase the membrane surface temperature and minimize the unpleasant TP effect [54]. Further thermal management strategies must be pursued to effectively reduce heat loss of metallic membranes and utilize the "Joule heating" advantage in MD and TOEC processes.

(ii) Vapor-gap membranes

Hydrophobic and nanoporous membranes, so-called vapor-gap membranes, are utilized in emergent methods to convert low-temperature heat energy into useful work. With nanodimentional cavities within the membrane structure, such specifically-designed membranes create and maintain a thin air gap, even under significant transmembrane hydraulic pressure [55]. Air is trapped within the pores when these membranes are submerged in two streams of water with different temperatures. Such temperature gradients assist hydrophobic membranes in overcoming the applied proper hydraulic pressure on the cold side and ultimately drive a vapor flux across the

membrane. Elimelech et al. analyzed the energy efficiency of vapor-gap membranes and demonstrated that nanoporous hydrophobic membranes could efficiently trap air even under hydraulic pressures up to 13 bar [25]. Power densities of up to 3.53 $\pm$0.29 W/m^2 can be obtained by circulating hot and cold water streams of 60 and 20 °C, respectively.

(iii) Nanocomposite membranes

Nanotechnology has played a critical role in facilitating the growth and improvement of membrane science. Membrane modifiers such as metallic NPs, carbon nanotubes, graphene, and organic metal frameworks have been used in membrane fabrication to obtain the desired structural and functional properties of membranes [26]. Metalloid and metal oxides-based nanoparticles are commonly utilized to improve membrane LEP, anti-fouling, and other characteristics of MD membranes [26]. Several single-element oxide NPs, including SiO_2, TiO_2, ZnO, and Al_2O_3, have been utilized to improve the permeation properties and wettability of MD membranes [56]. The focus has been mostly on TiO_2 NPs due to their high availability and exceptional physicochemical, antibacterial, and anti-fouling capabilities [57,58]. TiO_2 coating followed by fluorosilanization was done on the surface of PVDF membranes to reduce surface free energy and create multilevel roughness for MD application [59]. TiO_2-modified membranes showed no reduction in water flux after a 20 h fouling DCMD experiment with humic acid. Carbon-based nanomaterials, such as carbon nanotubes (CNTs), graphene, and graphene oxide, have also been used to fabricate MD nanocomposite membranes [60,61]. Membrane hydrophobicity and selectivity significantly improved by incorporating graphene oxides and metal oxide frameworks (MOFs) onto the surface or in the bulk of the membrane material [62]. Recent studies have shown that MOFs with clustered centers of aluminum (Al), zirconium (Zr), and iron (Fe) have excellent potential in water treatment processes [63]. Combined salinity and temperature gradients were used to extract electrical power in some research projects. The application of ultrasmall silica nanochannels (SNCs) in power harvesting through mutual salinity and temperature gradients was reported [64]. As an outstanding achievement, the salinity power output increased by 40% when a 10 K temperature gradient was applied in the TOEC process. Recently, a covalent organic framework (COF) based ion-selective membrane was developed to harvest energy from combined salinity and temperature differences [65]. **Figure 1.4.A** illustrates the chemical and morphological structures of the utilized materials as well as the different charge densities of the functional group on the synthesized COF. The bottom section of this figure presents the concept of electricity extraction from the thermos-

osmosis phenomenon. XRD patterns of different free-standing COFs are displayed in **Figure 1.4.B**. The prepared COFs were coated on the PAN substrate with a thickness of ~53–65 nm. **Figure 1.4.C** demonstrates the cross-sectional SEM image of the COF-$(SO_3Na)_1$/PAN membrane. The experimental results showed that the optimal membrane achieved a 97 W/m^2 power density using a 0.01/0.5 M salinity difference. **Figure 1.4.D** depicts the trend of extracted power density in different salinity gradients. Applying a 60 K temperature difference resulted in a large power density (231 W/m^2), which is 46 times larger than the commercial benchmark (5 W/m^2). The dependency of open-circuit voltage (V_{OC}) and short-circuit current (I_{SC}) on the temperature gradient across the membrane is exhibited in **Figure 1.4.E**.

1.2.2.3. Engineered TOEC processes

(i) Multistage TOEC

In a single-stage TOEC device, the heat of transported vapor within the condensation side is dissipated to the peripheral environment. Implementation of the single-stage TOEC on an industrial scale also requires very large spaces. Recently, Li et al. proposed a novel stackable TOEC system in which every working stage included two evaporation and condensation chambers [66]. Working plates and hydrophobic membranes separated the chambers from one another. The schematic illustration of such a multistage TOEC device is shown in **Figure 1.4.F**. Furthermore, **Figure 1.4.G** shows an experimental device with six sequential stages. The low-grade heat source increases the temperature of low-pressure water fluid in the furthest right evaporation chamber. The generated vapor can permeate through the membrane and reach the condensation chamber with a high-pressure water fluid. The higher temperature of the first condensation chamber is transmitted to the second adjacent evaporation chamber. This cycle repeats by increasing the number of working stages, leading to higher thermal efficiency. **Figure 1.4.H** displays the trend of power density and power efficiency increment by increasing the number of stages. Theoretical calculations revealed that a 30-stage TOEC device could obtain a power efficiency of 2.72% with a PD of 14.0 W/m^2 under 5.0 MPa hydraulic pressure.
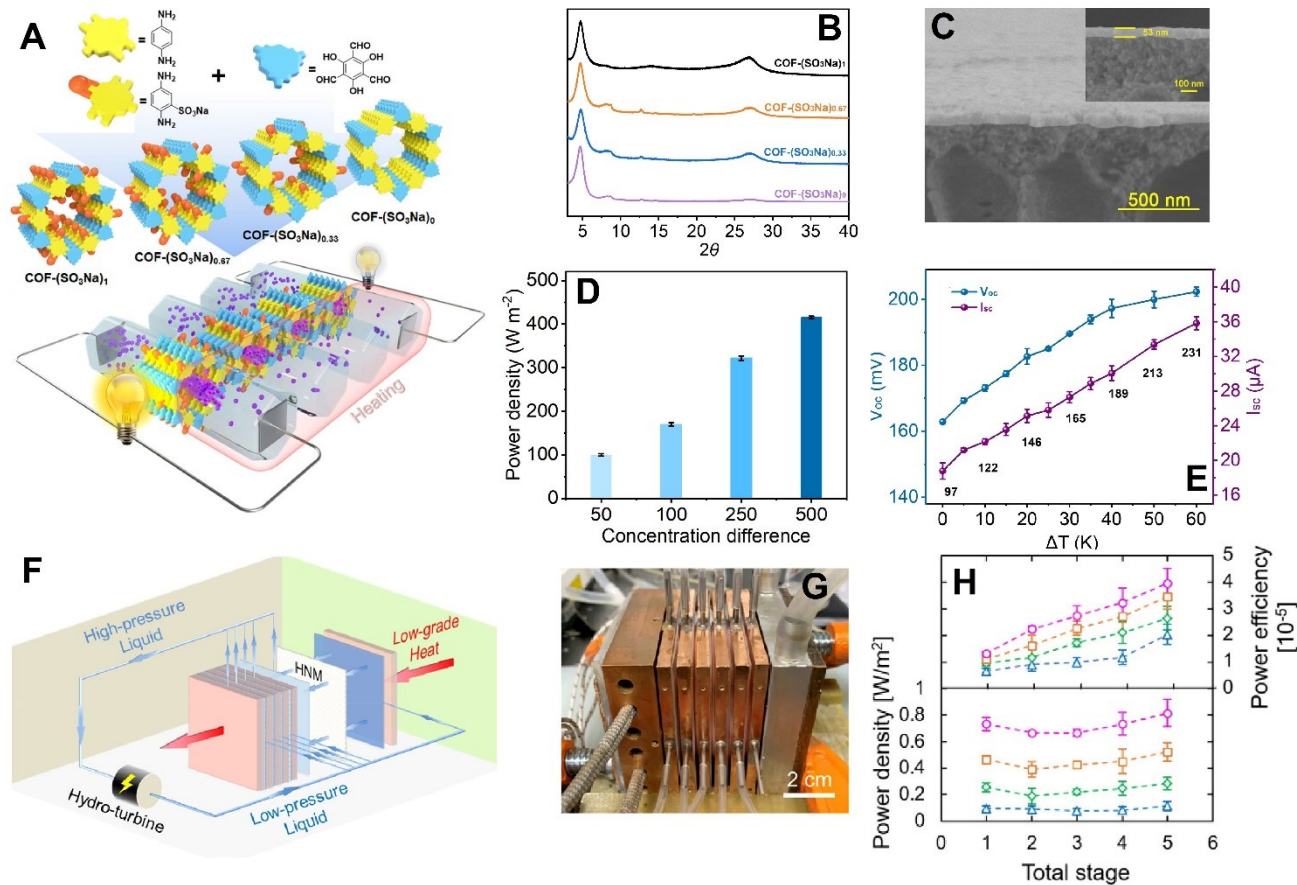
Figure 1.4. (A) Synthetic scheme of ionic COFs and a conceptual design for energy harvesting from salinity and temperature differences. (B) XRD patterns of free-standing COFs, (C) cross-sectional SEM image of COF-(SO$_3$Na)$_1$/PAN membrane, (D) power density trend versus salinity gradient, and (E) variations of V$_{OC}$ and I$_{SC}$ based on the temperature gradient. Figs. A-E are all adopted with permission from REF [65]. (F) Schematic illustration of the stack thermo-osmotic energy conversion system, (G) real image of the experiment device with six working stages, and (H) variation of power density and efficiency with increasing the number of stages in the stack TOEC design. Figs. F-H are all adopted with permission from REF [66].

(ii) Closed-loop design with heat recovery

To achieve the substantial flows required for power generation, membrane modules of considerable size should be implemented in large-scale TOEC systems. A closed-loop TOEC membrane module has great potential for full-scale implementation. This configuration demonstrates a higher performance in energy harvesting, where a heat exchanger is installed in the loop to recover the latent heat of vaporization and heat transfer through the membrane. The membrane module and heat exchanger operate continuously with countercurrent flow in this arrangement. The hot water vapor flows through the membrane module as the feed stream, and the

pressurized cold water acts as the permeate stream that enters the opposite end of the module [25]. Through the operation of closed-loop design, mass and heat transfer occurs through the membrane module from the hot feed stream to the cold permeate stream. Subsequently, a hydro turbine generates power by depressurizing the transmembrane current. The heat exchanger provides heat recovery for the system to harvest the heat transferred to the permeate stream and reduce the workload on the heat source. The heat exchanger efficiency required to achieve half of the maximum possible energy conversion efficiency is ~90%. Small reductions in the efficiency of heat exchangers can cause significant losses in energy production by the TOEC system [10]. The impact of low-efficiency commercially available heat exchangers can be offset by applying a higher hydraulic pressure on the cold side, in which case more power can be generated by passing each water molecule across the membrane. Modeling a closed-loop TOEC system with a heat exchanger efficiency of 90% and applied hydraulic pressure of 20 MPa showed that the energy conversion efficiency could reach 63%. Reducing the hydraulic pressure to 5 MPa could drop the same system's energy conversion efficiency to 29%. In a closed-loop TOEC system, pure water streams can be exploited on both sides of the membrane, which eliminates the membrane fouling challenges.

1.2.3. Research gaps

Even though the TOEC process holds promise for harvesting clean energy, existing research reveals critical gaps, shaping the focus of this thesis. A deeper understanding of fluid dynamics, transport phenomena, and molecular-level processes within thermo-osmotic systems is paramount. One substantial gap discerned in the literature revolved around the absence of an in-depth model for analyzing the performance of the TOEC process. While current models offer some insights into the principles and behavior of TOEC, there is a lack of a robust and integrated model that could simulate heat and mass transfer. Operational conditions and membrane properties intricately influence TOEC performance, necessitating further research to determine optimal conditions for maximizing energy conversion efficiency and power density.

The versatility of the TOEC system, adaptable through temperature adjustments, flowrates, applied pressures, and membrane properties, requires a precise model to predict and enhance operational modes and system performance. Such a model not only accelerates research but also mitigates the need for resource-intensive experimental analyses. Therefore, chapter 2 of this thesis plays a

pivotal role in addressing these critical research gaps by developing a comprehensive model for performance analysis.

Another discernible gap in the existing literature relates to the limited exploration of life-cycle analysis in the context of membrane synthesis for TOEC applications. While TOEC's environmental impact is acknowledged, assessing potential ecological consequences on a large scale remains unexplored. Research into cost reduction, efficiency enhancement, and operational optimization is indispensable. This gap in understanding sustainability considerations prompted the dedicated exploration in Chapter 3 of the thesis, conducting a detailed life-cycle analysis of membrane synthesis. By focusing on PVDF and PTFE membranes, this analysis aims to guide environmentally conscious material selection for TOEC technology. Bridging these gaps in the literature advances the understanding of TOEC processes and contributes significantly to the broader field of sustainable energy research. The integrated approach of this thesis, spanning from model development to life-cycle analysis, demonstrates a commitment to addressing multifaceted challenges in the quest for efficient and environmentally conscious energy generation.

1.2.4. Overview of model developments on the TOEC process

Central to the advancement of TOEC technology is the development of mathematical models that offer insights into its behavior, efficiency, and feasibility. This literature review surveys the current state of research and model developments related to the TOEC process, highlighting key findings, challenges, and potential future directions.

Lee's work [67] introduced the concept of pressure-retarded membrane distillation (PRMD), combining the principles of membrane distillation and pressure-retarded osmosis. . The process of PRMD is similar to that of TOEC. However, unlike the exclusive application of the TOEC process for energy harvesting, the closed-loop PRMD system can be used for the simultaneous desalination and power generation. Energetic and exergetic modeling equations were developed to investigate the feasibility of the closed-loop PRMD, and the effects of operating conditions and membrane parameters on the system were investigated. They reported that membrane parameters, particularly increasing contact angle and decreasing pore size, led to higher LEP and increased net energy production. Their results also demonstrated that the closed-loop PRMD system required low heat input and increased electrical energy production, offering a promising solution for desalination and energy harvesting from low-grade heat.

Chen et al. [68] delved into vapor pressure-driven osmosis (VPDO), developing a theoretical model to understand mass and heat transfer within VPDO. Working principle of VPDO is based on vapor transfer across a hydrophobic nanoporous channel, and is the same as the TOEC process. They used a generalized form of the Maxwell-Stefan equation combined with the dusty-gas model to simulate mass transfer through the hydrophobic nanoporous membrane. The study emphasized the importance of membrane properties, such as vapor permeability, and highlighted Knudsen diffusion dominance in mass transfer for VPDO. Their findings underscores the exponential increase in vapor flux with transmembrane temperature difference, emphasizing the unique advantage of VPDO in efficiently converting low-temperature heat sources to useful work. Moreover, they realized that thinner membranes exhibiting greater porosity and lower tortuosity lead to larger vapor permeabilities, significantly enhancing vapor flux and, consequently, improving power density performance in VPDO energy production. Membranes evaluated in the investigation are not specifically designed for VPDO's operating conditions, leaving room for advancement. Opportunities lie in the development of unique scaffold architectures that are highly porous without sacrificing sturdiness, potentially overcoming the tradeoff between membrane porosity and mechanical robustness.

Straub et al. [69] analyzed the energy efficiency and performance of TOEC using hydrophobic porous vapor-gap membranes. The study underscored the significance of membrane properties, heat exchanger efficiency, and optimal operating conditions in achieving high energy conversion efficiencies. In their simulation, they considered a TOEC system that uses counter-current flow in the membrane module and heat exchanger to improve the energy efficiency. They revealed that an optimized system with an operating pressure of 50 bar can achieve heat-to-electricity energy conversion efficiencies up to 4.1%, with hot and cold working temperatures of 60 and 20 °C, respectively. Moreover, they demonstared that the most important membrane properties for achieving high performance are high pressure resistance, asymmetric pore structure, high porosity, and a thickness ranging from 30 to 100 μm.

Shaulsky's work [70] explored asymmetric membranes with hydrophobic surfaces for membrane distillation and TOEC processes. A one-dimensional finite-element model (FEM) that integrates energy and mass balances was employed to assess the performance of the asymmetric membrane in MD and TOEC orientations. They demonstrated that the water vapor flow could be impeded by stagnant vapor or condensate accumulating in the principal layer, introducing resistance to mass

transfer. Nonetheless, this additional resistance to mass transport diminishes as the temperature gradient across the membrane decreases. Moreover, their modeling outcomes revealed a linear rise in the water vapor permeability coefficient concerning the temperature difference across the membrane in the MD orientation. In contrast, for the TOEC orientation, the water vapor permeability coefficient remained relatively stable across various temperature differences examined. The study highlighted the role of membrane structure in achieving high vapor flux while maintaining liquid entry pressure, which is crucial for efficient membrane distillation and TOEC. Xiao's research [71] introduced an open-loop freshwater and electricity cogeneration system using a hydrophobic, porous membrane. This innovative system implemented thermal-osmotic energy conversion and thermal-osmotic desalination simultaneously. They utilized Secant method for simulating the heat and mass transfer process in the membrane module. The study explored net power output, energy efficiency of power generation, and cost-effectiveness, identifying membrane properties and operating conditions as key factors in improving energy efficiency and reducing water production costs. They revealed that improvements in LEP and permeability coefficient and reducing the thermal conductivity of the membrane are the key to enhancing the application prospect of the system.

These studies emphasize the growing interest in mathematical modeling and the potential of TOEC technology as a sustainable energy solution. They address various aspects of TOEC, including energy efficiency, membrane properties, and system design, providing insights into its feasibility and practicality. Gaps in the literature include the need for more comprehensive modeling to accurately predict the performance of a TOEC system that can incorporate the impact of elevated applied pressures on the membrane surface, inducing membrane surface compaction. Additionally, there is a call to optimize membrane properties, explore scalable and economically viable TOEC systems, and analyze environmental implications associated with manufacturing specialty TOEC membranes.

1.2.5. Overview of life-cycle assessment (LCA)

Life Cycle Assessment (LCA) is a method for evaluating the environmental impacts of a product or service over its entire life cycle, aiding businesses, policymakers, and organizations in making sustainable decisions. LCA can support marketing efforts by substantiating environmental claims and meeting consumer demand for eco-friendly products. It enables the quantification of key

environmental impacts such as greenhouse gas emissions, carbon emissions, water use, and energy consumption [72]. The LCA process generally consists of four phases:

1. *Definition of Goal and Scope:* Establishing the parameters of analysis and the depth of the study [73].

2. *Life Cycle Inventory (LCI):* Collecting data on inputs and outputs of materials and energy flows throughout the product's life cycle [74].

3. *Life Cycle Impact Assessment (LCIA):* Evaluating the significance of impacts by quantifying emissions and assessing potential ecological and human health effects at each stage [72].

4. *Interpretation*: Summarizing LCIA findings and providing recommendations for reducing environmental impacts [75]

Different life cycle models can be used based on the stages of interest or data availability. Some common models include "cradle-to-grave", which analyzes a product's impact from the sourcing of the raw materials to the disposal of the product, and "gate-to-gate", which focuses on one value-added process in the production chain. Other models like "well-to-wheel" are used for specific requirements, such as evaluating transport fuels and vehicles [72].

Lawler et al. [76] conducted a life cycle assessment model for reverse osmosis membrane manufacturing and discussed end-of-life options. They revealed that membrane reuse over one year is more environmentally favorable than landfill, and transportation distance and lifespan play a significant role in reuse viability. Furthermore, they demonstrated the relative environmental burden for 9 difference impact categories, and they found that the production and transportation of an 8″ RO element contribute 87 kg CO_2-e emissions to the atmosphere. In the context of product development, Firouzjaei et al. [74] presented the first life-cycle assessment on the MXene nanomaterials family. They provided an inventory of the material, energy, and waste flows for the synthesis of $Ti_3C_2T_x$ MXene. Furthermore, they investigated the CED and environmental implications of $Ti_3C_2T_x$ synthesis based on various factors such as precursor production, selective etching, delamination processes, laboratory location, energy mix, and raw material type. Their findings showed that laboratory electricity usage for the synthesis processes accounts for >70% of the environmental impacts, and it cleared the gap between real-life products in use and laboratory-scale MXene. We believe such studies could help the development of new membranes and products in this category to better fit the industrial need.

LCA is a complex tool, and accurate, consistent data collection is crucial. Several software programs, including OpenLCA, facilitate LCA implementation [74]. This study utilized a comprehensive cradle-to-grave life cycle analysis with OpenLCA to assess the environmental impacts and cumulative energy demands associated with manufacturing membranes for the TOEC process.

1.3 Thesis objectives

This thesis aims to pioneer the development of a robust mathematical model for simulating heat and mass transfer in the TOEC process, addressing identified gaps in existing research. The objective is to introduce a novel approach enabling accurate prediction of various factors, including permeate flux, energy efficiency, power density, and temperature polarization. The theoretical model conducts a sensitivity analysis on key parameters, establishing an optimized design map for membrane properties and operational conditions to enhance energy efficiency and power density. This study was executed through several distinct phases: (i) exploring heat and mass transfer mechanisms, (ii) applying foundational principles to model the TOEC process, and (iii) formulating a groundbreaking mathematical model inspired by the Effectiveness-Number of Transfer Units ($\in$-NTU) method. Then, the accuracy and reliability of the theoretical predictions were validated against experimental values, ensuring the model's precision.

In addition to TOEC process modeling, the thesis focuses on membrane manufacturing for TOEC, evaluating environmental impacts and energy demands. This investigation conducts a comprehensive life cycle assessment covering small-scale laboratory production and large-scale manufacturing of vital TOEC membranes. The study addresses a significant knowledge gap, providing insights into the energy demands and environmental impacts of manufacturing PTFE and PVDF membranes. These discoveries guide decision-makers, facilitating informed choices for sustainable practices and exploring eco-friendly alternatives.

1.4 Thesis outline

The first chapter delves into the fundamental aspects of the TOEC process and its significance. This chapter unfolds the challenges and opportunities in developing the TOEC process. Emphasis

is placed on exploring existing literature, identifying critical research gaps, and introducing TOEC model developments and life-cycle assessment methodologies. The chapter concludes by clearly defining the objectives and scope for subsequent chapters.

Chapter 2 elucidates core principles governing heat and mass transfer mechanisms within the TOEC process. It develops a robust mathematical model based on the ε-NTU method to predict and assess system performance metrics, including permeate flux, energy efficiency, power density, and temperature polarization. Moreover, the chapter compares various membranes to optimize the TOEC process regarding energy efficiency, power density, and temperature polarization.

Chapter 3 shifts focus to membrane manufacturing for TOEC applications, evaluating both small-scale and large-scale fabrication to comprehend environmental impacts and energy demands. Insights from this analysis pave the way for developing sustainable and eco-friendly membrane fabrication processes.

The last chapter provides primary findings and contributions, thoroughly discussing implications for industry adoption, future research directions, and potential avenues for further exploration.

2. Model development for performance analysis of the TOEC process

2.1 Introduction

The United Nations projects that the world population will increase from 7.7 billion in 2019 to more than 9.7 billion in 2050 [77]. This substantial population growth will inevitably lead to an increase in global energy demand. As more individuals and urban areas become connected to the global energy grid, the strain on resources becomes unavoidable. One crucial resource affected is water, as traditional power generation plants typically require a significant amount of water in various forms. Therefore, it is imperative to prioritize low-cost, sustainable, and efficient energy extraction methods to support this growing trend while mitigating the impact on water and other resources. As non-renewable energy sources begin to fade, harvesting renewable energy becomes of utmost importance.

The field of low-grade waste heat energy recovery is gaining traction, focusing on generating power from hot fluid streams below 150 °C [78,79]. This form of low-grade heat is abundant globally and can be harnessed from geothermal and industrial sources, offering significant potential for electricity generation [10,25,80]. The amount of low-grade waste heat produced by industrial facilities in the USA alone is roughly equivalent to the country's entire energy consumption in 2013 (~2.9×10^4 TWh) [4]. The waste heat potential of primary energy sectors in China, the world's largest energy consumer, is estimated to range from 15% to 40% of the total fuel input [4]. A suitable technology for converting low-grade heat to electricity must produce high power densities (per unit area or volume) while being scalable and cost-effective. However, current technologies cannot efficiently extract energy from heat sources with variable heat output or small temperature differences between the outlet and the environment [4,81]. Therefore, significant technological advancements are required to fully tap into the abundant energy available from low-grade heat sources. Huang et al. [82] developed a hybrid system that combines membrane distillation with a microfluidic power generator. This inventive coupling enabled the simultaneous generation of clean water and power using low-grade heat sources. Based in their study, operating at a temperature difference of 40 °C, the hybrid system achieved a freshwater production rate of 13.4 kg m^{-2}h^{-1}, while generating electricity with an output of 147 µWm^{-2}. Organic Rankine cycles

(ORCs) and solid-state thermoelectrics (TEs) have received significant attention, but the power densities achieved by these methods have not been cost-effective or quantitatively substantial [4,83–86]. While solid-state thermoelectric systems have primarily targeted low-temperature ranges but are expensive and have achieved limited efficiencies, typically below 12% of the Carnot efficiency [4,85]. An alternative approach known as thermally regenerative electrochemical cycles (TRECs) offers the potential to convert low-grade thermal energy into electricity by utilizing voltage differences induced by temperature disparities [4,87]. However, the main challenge of TRECs lies in achieving high efficiency and scalability.

Thermo-osmotic energy conversion (TOEC) is an emerging process that efficiently extracts energy from low-grade heat sources [10,70]. By utilizing a temperature gradient, TOEC induces a partial vapor pressure difference across a hydrophobic membrane. This pressure gradient drives the vapor from the hot feed side through the membrane's pores to the cold permeate side [10]. The movement of water from the hot feed side to the permeate side of the membrane results in excess fluid in the cold reservoir, generating a pressurized flow that can be harnessed to drive a turbine and generate electricity [70]. Remarkably, this process can operate effectively with only a minimal temperature gradient between aqueous solutions. Luo et al. [88] have integrated the TOEC process with an electrokinetic module to simultaneously harness low-grade heat energy to generate electricity and collect the resulting freshwater. Notably, after continuous operation at a temperature differential of 50 °C, their prototype device achieved an output power density of 1.12 Wm^{-2} and a freshwater production rate of 18.46 kg $m^{-2}h^{-1}$.

Despite the initial promise of the TOEC system, it is still in the early stages of development, and several challenges must be overcome before scaling it up to efficiently convert low-grade heat into electricity. One such challenge is membrane wetting, which occurs when the hydraulic pressure applied to the membrane exceeds the liquid entry pressure (LEP), causing water to penetrate the hydrophobic membrane in liquid form and render it wet [65,89–91]. Controlling membrane wetting requires a high LEP, but reducing the membrane pore diameter to increase LEP sacrifices vapor transport within the pore. This creates a dilemma because a high vapor flux necessitates a lower LEP, making the membrane more prone to wetting [27,70,92]. The performance of the TOEC process is also influenced by temperature polarization (TP). TP forms a boundary layer between the feed and permeate sides of the membrane and the bulk fluid, causing thermal

resistance and a temperature difference between the membrane surface and the bulk fluid. This reduction in thermal driving force subsequently lowers the permeate flux [8,93].

Another challenge in the TOEC process is membrane compaction resulting from the hydraulic pressure applied to the permeate side. Although the applied pressure on the permeate side has minimal impact on vapor flow driven by a temperature gradient, it has been observed that membrane compaction leads to a significant drop in water flux in previous studies [12,25,67,94]. Straub et al. [25] investigated the effect of compaction on membrane performance and found that the PTFE membrane compacts under higher hydraulic pressures, resulting in decreased vapor permeability. Lee et al. [67] simulated the impact of membrane compaction by raising the membrane resistance, which ultimately reduced vapor flux. Nevertheless, most previous studies evaluating the TOEC process focused on operating conditions, membrane properties, and module design, neglecting the effects of membrane deformation under higher applied pressures on performance metrics such as power density, energy efficiency, and thermal efficiency.

In the literature, several studies have focused on modeling Membrane Distillation (MD) using the effectiveness-number of transfer units (ε-NTU) method [7,8,95]. However, there have been no known studies that have specifically employed the ε-NTU method for the modeling of TOEC. This indicates a research gap where further investigation is needed to explore the applicability of the ε-NTU method in TOEC modeling. By incorporating the ε-NTU method, we are able to accurately analyze the complex interplay of temperature variations along the membrane length and across the membrane thickness, providing a more comprehensive understanding of the TOEC performance. Furthermore, the majority of previous studies on TOEC modeling have primarily focused on theoretical approaches, resulting in a lack of reasonable agreement between the modeling and experimental results. This discrepancy suggests that the existing models may not fully capture the intricate mechanisms involved in TOEC. Therefore, further research is necessary to refine and improve the existing models, considering factors such as fluid dynamics, heat transfer, mass transfer, and membrane deformation to better align the modeling predictions with experimental results and enhance the accuracy and reliability of TOEC modeling. This study breaks new ground by considering the impact of membrane compaction on the TOEC system performance. By accounting for membrane compaction, our model offers a more realistic assessment of power density, energy efficiency, and thermal efficiency. Finally, this study presents the first comprehensive prediction of the TOEC system's performance under various conditions. Notably,

the experimental results obtained from our system are in excellent agreement with the modeling results, demonstrating the effectiveness of our approach. By combining the novel utilization of the ε-NTU method and considering membrane compaction, this research significantly advances the understanding and potential implementation of the TOEC process for efficient low-grade heat-to-electricity conversion.

2.2 Methods and Theory

2.2.1 Process description

A typical TOEC system utilizes a hydrophobic nanoporous membrane, creating an air gap to separate the cold and hot streams of liquid water [25]. While exploring different liquids and membranes in the TOEC system is theoretically possible, most studies have focused on hydrophobic membranes and water as the working medium [25,96]. When immersed in water, the hydrophobic membranes trap air within their pores, establishing a barrier between the two reservoirs [4,97,98]. The TOEC process primarily relies on thermoosmosis, which involves fluid flow through a membrane driven by temperature differences [99,100].

Figure 2.1. demonstrates the process wherein liquid water evaporates from the membrane's hot side and condenses on the cold side after passing through the membrane pores as vapor. The temperature disparity across the membrane and the resulting relative vapor pressure difference facilitates a net vapor flow from the hot side to the cold side. This thermo-osmotic phenomenon transports fluid from a reservoir at ambient pressure to a reservoir at a higher hydrostatic pressure, effectively converting thermal energy into mechanical work. The pressurized fluid flow on the membrane's cold side can be depressurized using a hydro-turbine, thereby generating electrical power. The flexibility of the TOEC system allows for the utilization of a wide range of source temperatures since the driving force stems from a partial vapor pressure differential between the air and liquid interfaces on each side of the membrane. Consequently, this process operates efficiently even with variable-temperature sources [10].
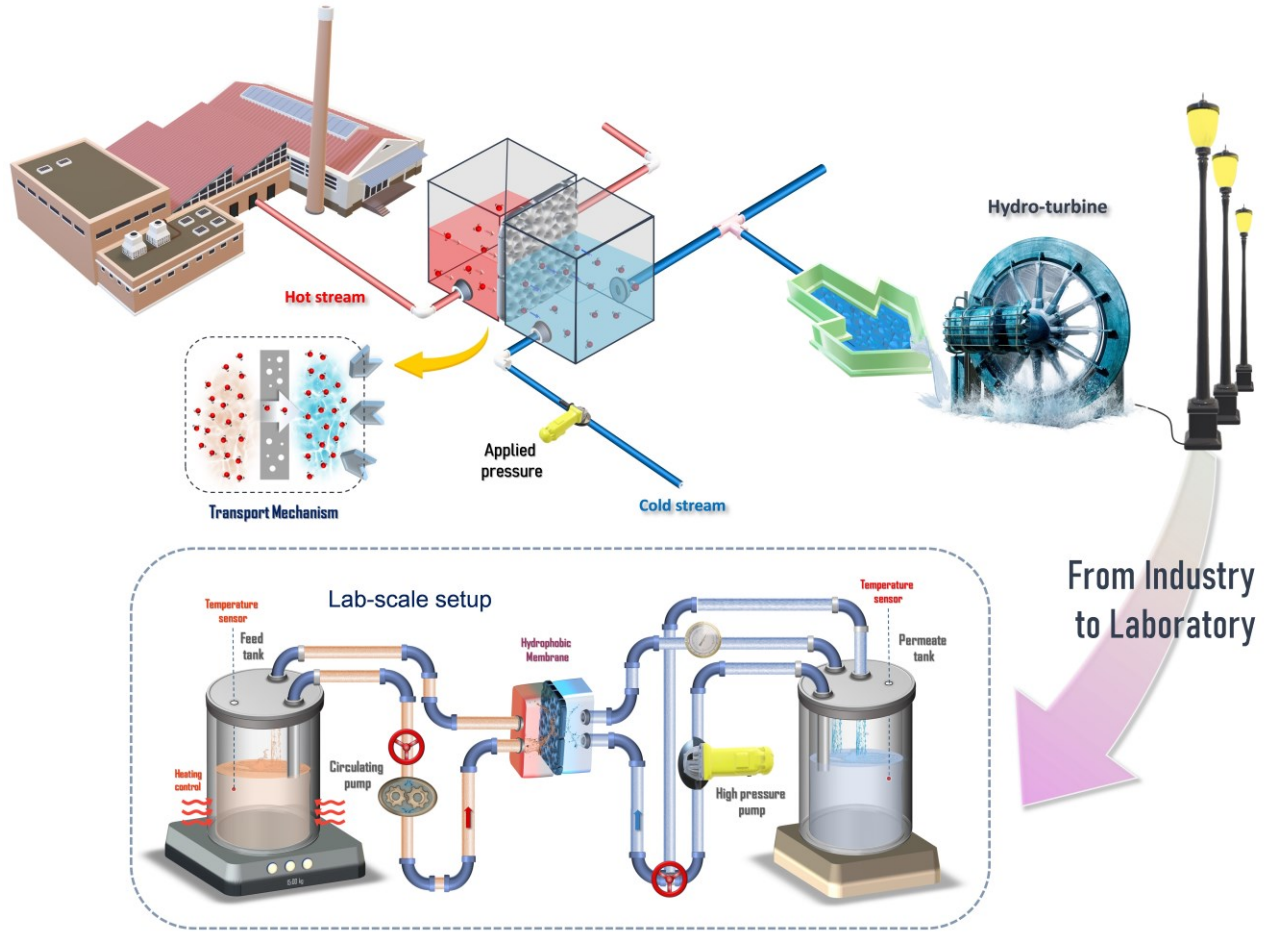
Figure 2.1. Schematic illustration of a TOEC system across a hydrophobic nanoporous membrane. In a standard TOEC system, the heated liquid water from the feed tank enters the membrane cell. Subsequently, the liquid water undergoes evaporation on the feed side of the membrane, allowing the vapor molecules to traverse the hydrophobic membrane and ultimately condense on the permeate side. Electricity can be generated by applying hydraulic pressure on the cold side and regulating the fluid flow using a hydro turbine.

2.2.2 Mass transfer

During the TOEC process, the vapor is transported across hydrophobic membrane pores. This transport is driven by the vapor pressure difference between the cold and hot streams [67]. The mass flux through the membrane (J_w) can be determined using the membrane's permeability coefficient (B_M) and the vapor pressure difference (ΔP_v) across the membrane, as expressed below [10]:

$$J_w = B_M\left[P_{v,h}\left(T_{H,m}, 0\right) - P_{v,c}\left(T_{C,m}, P_h\right)\right] \tag{2.1}$$

The P_v depends on the hydraulic pressure corresponding to the surface temperatures of the hot $(T_{H,m})$ and cold $(T_{C,m})$ sides of the membrane. In a TOEC process, the hot side does not experience hydraulic pressure, so its vapor pressure solely relies on the feed temperature. This can be calculated using the Antoine equation [10,101]:

$$\log_{10}(P_{v,h}) = A - \frac{B}{C + T_{H,m}} \tag{2.2}$$

where $T_{H,m}$ is the membrane surface temperature on the hot side, and three constants (A, B, and C) are provided in the literature [101]. The vapor pressure on the cold side, denoted as $P_{v,c}$, can be calculated using the modified Kalvin equation as follows [102]:

$$\ln\frac{P_{v,c}}{p_{sat}} = \frac{P_h \times V_m}{RT_{C,m}} \tag{2.3}$$

where p_{sat} represents the equilibrium vapor pressure at ambient pressure and the surface temperature of the cold side $(T_{C,m})$, which can be estimated using the Antoine equation. P_h is the applied hydraulic pressure on the cold side, V_m is the molar volume of liquid water, and R is the universal gas constant.

The vapor permeability coefficient of the membrane is influenced by various factors, including the membrane properties, surface temperatures on both sides of the membrane, and the specific type of diffusion that takes place within the membrane pores. There are three main categories of diffusion: (1) Knudsen diffusion, (2) molecular diffusion, and (3) transitional diffusion, which is a combination of Knudsen and molecular diffusion [8]. The Knudsen number (K_n) determines the diffusion type, and is obtained using the following equations [8]:

$$K_n = \frac{\lambda}{d_{pore}} \tag{2.4}$$

$$\lambda = \frac{K_B T_m}{\sqrt{2}\pi P_m \sigma^2} \tag{2.5}$$

where λ is the mean free path of the transported vapor molecules across the membrane, d_{pore} is the membrane pore size, K_B is the Boltzmann constant, T_m is the average surface temperatures of the feed and permeate side, P_m is the mean pressure within the membrane pores, and σ is the collision diameter of water molecules, which is equal to 2.641×10^{-10} m. The pore size plays a crucial role in determining the type of diffusion. When membranes possess nanoscale pores, their Knudsen numbers tend to be large, resulting in Knudsen flow dominating the fluid flow.

Conversely, membranes with micrometer-sized pores exhibit lower Knudsen numbers, causing molecular diffusion to be the predominant mode of flow. When $K_n > 1$, mass transport through the pores is primarily governed by Knudsen flow, and the following equation represents the permeability coefficient of the membrane:

$$B_M = \left(\frac{2\varepsilon r}{3\delta\tau}\right)\sqrt{\frac{8M_w}{\pi R T_{avg,m}}} \tag{2.6}$$

where ε is the porosity, r is pore size, δ is the membrane thickness, τ is the tortuosity, M_w is the molecular weight of water, and $T_{avg,m}$ is the average temperature of membrane surfaces at feed and permeate sides. If $K_n < 0.01$, molecular diffusion is the primary contributor to the mass transfer through the pores. In this case, the membrane's permeability coefficient can be estimated using the following equation [8,103]:

$$B_M = \left(\frac{M_w \varepsilon P D}{R T_{avg,m} \delta\tau P_{air,pore}}\right) \tag{2.7}$$

where P is the total pressure inside the pores, D is the water diffusion coefficient, and $P_{air,pore}$ is the air pressure in the membrane pores. The value of PD can be calculated as follows [104,105]:

$$PD = 1.895 \times 10^{-5} T_{avg,m}^{2.072} \tag{2.8}$$

If $1 > K_n > 0.01$, the mass transfer results from a combination of Knudsen flow and molecular diffusion. In this situation, the permeability coefficient of the membrane can be calculated by the following equation [8,106]:

$$B_M = \left[\left[\left(\frac{2\varepsilon r}{3\delta\tau}\right)\sqrt{\frac{8M_w}{\pi R T_{avg,m}}}\right]^{-1} + \left[\left(\frac{M_w \varepsilon P D}{R T_{avg,m} \delta\tau P_{air,pore}}\right)\right]^{-1}\right]^{-1} \tag{2.9}$$

Although the applied pressure on the permeate side has little impact on the vapor flux, earlier studies [12,25,94] have observed a significant decrease in flux due to membrane compaction. This compaction-induced reduction in membrane permeability leads to lower vapor flux at higher operating pressures. Experimental data [25] demonstrated that the net vapor flow decreases as the pressure on the cold stream increases. To model the effect of membrane compaction, we introduce a compaction factor (r_{comp}) as an additional parameter in the permeability coefficient equation. This factor signifies how an increase in hydraulic pressure on the cold side reduces the

permeability coefficient and consequently affects the vapor flux. The equation below captures the impact of compaction on membrane permeability [67]:

$$B_{M,real} = \frac{B_{M,apparent}}{1 + r_{comp}} \qquad (2.10)$$

where $B_{M,apparent}$ is the apparent permeability coefficient calculated based on Equations. 2.6, 2.7, or 2.9. The $B_{M,real}$ is the real permeability coefficient that must be used to find the vapor flux by Equation 2.1. According to the literature, there is an exponential relation between the compaction factor and the applied hydraulic pressure on the membrane [107]. By examining relevant experimental data available in the literature [25], we could derive an equation that correlates the compaction factor with the applied hydraulic pressure:

$$r_{comp} = A \times \exp(B \times P_h) + C \qquad (2.11)$$

A, B, and C are constants that can be determined based on experimental results. For the PTFE membrane with a pore size of 20 nm, the corresponding values of these constants are 0.022, 3.8×10^4, and -0.022, respectively. The temperature gradient between the hot and cold sides of the membrane serves as the driving force for the TOEC process. This temperature difference changes vapor pressure across the membrane, facilitating vapor flow through the pores. The following equation can be employed to estimate the hydraulic pressure generated by thermo-osmosis at a specific temperature difference [10]:

$$P_{TO} = \frac{Q_M}{V_M}\left(1 - \frac{T_C}{T_H}\right) \qquad (2.12)$$

where P_{TO} is the hydraulic pressure that can be produced from a given temperature difference, Q_M is the molar vaporization enthalpy of the working fluid, V_M is the molar volume of the working media, and T_C and T_H are the surface temperatures of the membrane on the cold and hot sides, respectively. It has been reported in the literature that even 1 °C transmembrane temperature gradient can potentially result in a significant increase in hydraulic pressure, ranging from 6 to 7 MPa [66]. Using Equation 12 and considering feed water temperature of 60 °C and permeate water temperature of 20 °C, the potential pressure increment would amount to 2700 bar, demonstrating the promise of energy harvesting from the TOEC process. To effectively harness these substantial pressure increments, it is crucial to apply hydraulic pressure close to the generated potential pressure corresponding to the temperature gradient. However, in order to apply high pressures on

the condensation side of the membrane, the pore size must be sufficiently small to create an adequate capillary force that prevents the penetration of liquid water into the bulk structure of the membrane [10]. In other words, if the applied pressure exceeds the LEP of the membrane, water will permeate through the pores, leading to wetting of the membrane. The LEP of a membrane can be estimated using the following equation [108]:

$$LEP = \frac{-2\beta\gamma\cos\theta}{r_{max}} \tag{2.13}$$

where β is a geometric pore coefficient ($\beta = 1$ for cylindrical pores), γ is the liquid surface tension, θ is the contact angle, and r_{max} is the maximum pore radius.

2.2.3 Heat transfer

Heat is transferred across the membrane through two mechanisms: heat conduction within the membrane material and heat convection facilitated by water vapor flowing through the membrane pores. Hence, the total heat transfer across the membrane can be determined using the following equation [10]:

$$q = J_w h_{vap} + \frac{K_c}{\delta}\left(T_{H,m} - T_{C,m}\right) \tag{2.14}$$

where h_{vap}, and K_c are the enthalpy of vaporization and the membrane's thermal conductivity, respectively. Both the thermal conductivity of the polymer and air in the pores should be used to estimate the thermal conductivity of the membrane [109]. The overall heat transfer coefficient, which is based on the bulk feed and permeate temperatures, can be calculated by this equation:

$$U = \frac{1}{\left[\frac{1}{h_f}\right] + \left[\dfrac{1}{\left[\frac{K_c}{\delta}\right] + \left[\dfrac{J_w h_{vap}}{T_{mf} - T_{mp}}\right]}\right] + \left[\frac{1}{h_p}\right]} \tag{2.15}$$

The temperature at the liquid/vapor interface on both sides of the membrane affects the vapor flux and heat flux [110]. Temperature polarization in the thermal boundary layers on either side of the membrane causes the temperature difference at the interface to be smaller compared to the bulk fluid [10]. This temperature polarization substantially reduces the thermal driving force and the resulting permeate flux. Temperature polarization is defined as the ratio of the temperature difference at the membrane liquid-vapor interface (T_m) to the temperature difference in the bulk fluid (T_b) on the feed and permeate sides. It can be quantified as follows [8]:

$$\text{Temperature polarization } coefficient\ (TPC) = \frac{T_{mf} - T_{mp}}{T_{bf} - T_{bp}} \tag{2.16}$$

The temperatures at the membrane liquid-vapor interface at the feed and permeate sides are calculated by the following equations [25]:

$$T_{mf} = T_{bf} - q/h_f \tag{2.17}$$

$$T_{mp} = T_{bp} + q/h_p \tag{2.18}$$

where h_f and h_p are the convection heat transfer coefficients of the boundary layer on the feed and permeate sides of the membrane, respectively. To ensure the successful implementation of the TOEC process, careful consideration must be given to both the energy and thermal efficiency of the system. Energy efficiency is determined by dividing the work output by the thermal energy input. Meanwhile, thermal efficiency plays a vital role in assessing the effectiveness of heat transfer across the membrane. It can be defined as the ratio of heat transferred across the membrane by convection (the latent heat of vaporization) to the total heat transfer across the membrane [8,10]:

$$\eta_{th} = \frac{J_w h_{vap}}{J_w h_{vap} + \frac{K_c}{\delta}\left(T_{H,m} - T_{C,m}\right)} \tag{2.19}$$

2.2.4 Process modeling

In this study, a theoretical model was developed to analyze the TOEC module by applying mass and heat transfer principles. The control volume surrounding the TOEC cell is depicted in **Figure 2.2**. The temperature distribution on the membrane surface was calculated using the ε-NTU method. We utilized MATLAB programming software to simulate the TOEC process, employing the equations above. By employing non-dimensional parameters derived from counter/parallel-flow heat exchangers [8], the ε-NTU model enabled us to feasibly simulate the heat and mass transfer in the TOEC process.

The modeling assumptions are outlined as follows: (1) The heat dissipation from both the membrane module and the flow systems to the surrounding environment is considered negligible due to effective insulation in our experimental setup, minimizing heat loss. (2) The impact of viscous flow on mass transfer through membrane pores is deemed negligible, supported by the

29

presence of air within the pores. (3) Uniform cylindrical channels are presumed for the membrane pores, with the pore diameter serving as a key modeling input influencing TOEC performance.

To accurately resolve the heat and mass transfer within the TOEC system, we combined finite-difference and ε-NTU approaches. The ε value represents the ratio of the actual heat transfer rate to the maximum heat transfer rate of a heat exchanger, while NTU denotes the heat transfer capacity. Since the parameters at the outlet of the cold and hot streams are unknown, employing the ε-NTU approach allows for precise prediction of the outlet temperatures [8]. In this technique, assumptions are made regarding the inlet streams of the heat exchanger, and the ε-NTU technique is utilized to determine the outlet temperatures of the heat exchanger.
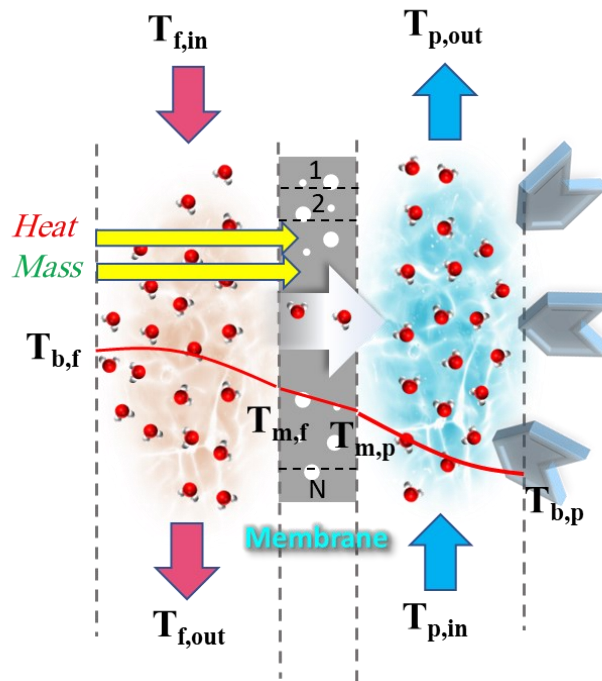
Figure 2.2. Schematic representation of heat and mass transfer across the membrane in the TOEC system

The mathematical algorithm employed to predict the performance of the TOEC process is illustrated in **Figure 2.3**. The modeling inputs are membrane properties, physical properties of fluids, module geometry, and operating conditions. The outputs include vapor flux, temperature polarization effect, energy efficiency, thermal efficiency, and power density. Initially, the input values and bulk temperatures of the feed and permeate were used to determine the fluid velocity,

Reynolds (Re), Prandtl (Pr), and Nusselt (Nu) numbers, along with the heat transfer coefficients (h_f,h_p).

We assumed the bulk temperatures (T_{bf} and T_{bp}) were the same as the inlet temperatures ($T_{f,in}$ and $T_{p,in}$) for the feed and permeate streams. Using the ∈-NTU equations in **Table 2.1** and the counter-current flow, we determined the outlet temperatures ($T_{f,out}$ and $T_{p,out}$). Next, the temperature profile along the membrane surface was calculated by dividing it into a finite number of elements. During the main loop, the estimated outlet permeate temperature ($T_{p,out}$) from the previous step is utilized as the initial guess for the permeate stream's inlet temperature in the first element. We also used a parallel flow pattern to continue the calculations. Using the ∈-NTU method for parallel flow, we calculated the outlet temperatures for each element. This iteration continued until the outlet permeate temperature for the last element (N) matched the main inlet permeate temperature. Finally, after the iteration converged, we calculated the permeate flux, energy efficiency, TPC, thermal efficiency, and power density.
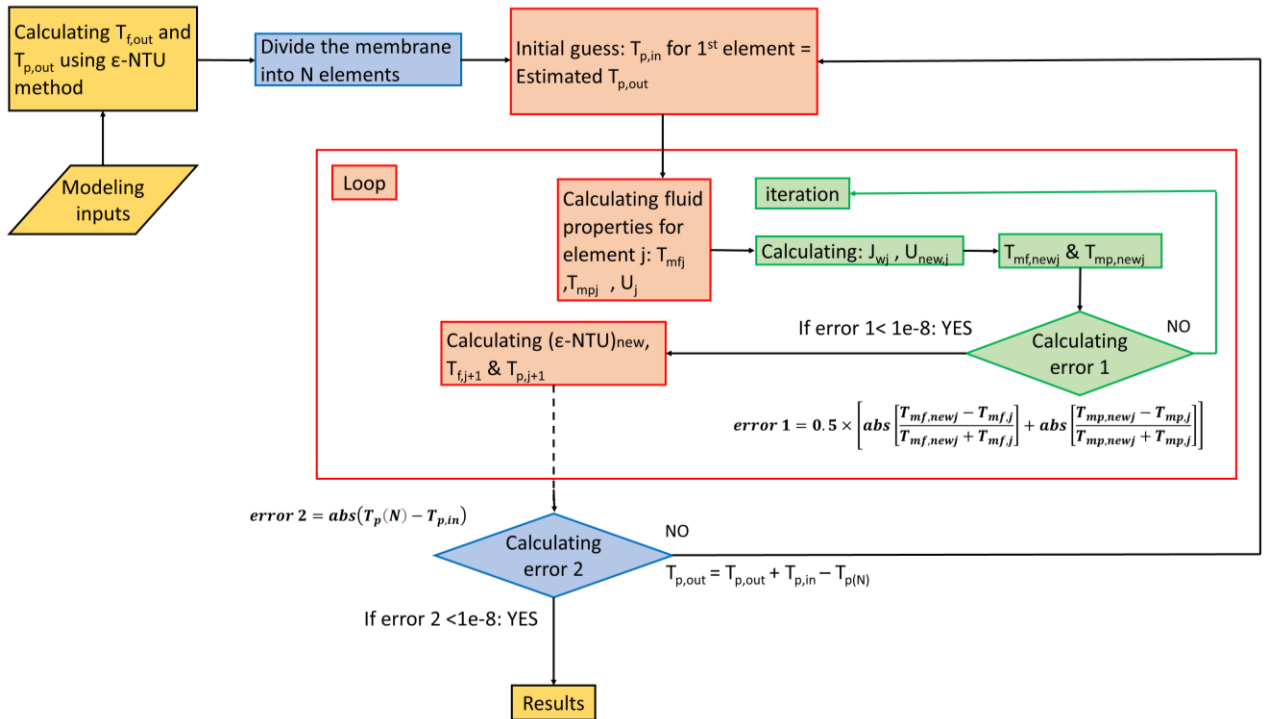
Figure 2.3. The mathematical algorithm used to predict the TOEC performance by MATLAB software.

Table 2.1. Equations for calculating the outlet temperature utilizing the ∈-NTU technique.

$$C_p = \dot{m}_p c_{p,p} \tag{2.20-a}$$

$$C_f = \dot{m}_f c_{p,f} \tag{2.20-b}$$

$$C_{min} = Min(C_f, C_p) \tag{2.21-a}$$

$$C_{max} = Max(C_f, C_p) \tag{2.21-b}$$

$$C_r = \frac{C_{min}}{C_{max}} \tag{2.22}$$

$$NTU = \frac{U(membrane\ area)}{C_{min}} \tag{2.23}$$

$$If\ C_r = 1: \ \varepsilon = \frac{NTU}{NTU+1} \tag{2.24-a}$$

$$If\ C_r < 1: \ \varepsilon = \frac{1-\exp{(-NTU(1-C_r))}}{1-C_r\exp{(-NTU(1-C_r))}} \tag{2.24-b}$$

$$\varepsilon = \frac{Q}{Q_{max}} \tag{2.25}$$

$$Q = C_p\ (T_{p,out} - T_{p,in}) \tag{2.26}$$

$$Q_{max} = C_{min}\ (T_{f,in} - T_{p,in}) \tag{2.27}$$

$$T_{f,out} = T_{f,in} - ((T_{p,out} - T_{p,in})/C_r) \tag{2.28}$$

$$T_{p,out} = T_{p,in} + Q/C_c \tag{2.29}$$

2.2.5 Simulation parameters and operating conditions

We comprehensively analyzed the TOEC system's performance using two commercial hydrophobic membranes: polytetrafluoroethylene (PTFE) and polyvinylidene difluoride (PVDF). **Table 2.2** presents the structural properties of these membranes. PTFE 0.45 μm, PTFE 0.2 μm, and PVDF membranes were acquired from Sterlitech Company and PTFE 0.02 μm membrane was obtained from Pall Corporation. The modeling parameters can be divided into two categories: modeling inputs and modeling outputs. The modeling inputs encompass membrane properties (such as pore size, porosity, tortuosity, membrane thickness, active surface area, and thermal conductivity), module geometry, operating conditions (including bulk temperatures and flowrates), and physical properties of fluids in the feed and permeate streams [8]. Throughout the investigation, the bulk temperature ranged from 30 °C to 90 °C, while the flowrate on both sides of the membrane varied between 0.2 and 0.8 LPM. On the other hand, the modeling outputs consisted of vapor flux, thermal efficiency, energy efficiency, temperature polarization effect, power density, and heat transfer rates.

Table 2.2. Structural properties of the membranes used in the present study. The properties of the membranes were obtained from the suppliers' manuals.

Membrane	Pore size (µm)	Porosity (%)	Water Contact Angle (°)	Thickness (µm)
PTFE	0.45	83	123	100
PTFE	0.2	81	135.5	100
PVDF	0.3	80	95	150
PTFE	0.02	77	137.4	43

2.3 Results and Discussion

In this section, we compared and evaluated the performance of a TOEC process using four different membranes with various pore sizes. The modeling and experimental studies were done on PTFE membranes with 0.45 µm, 0.2 µm, and 20 nm pore sizes and a PVDF membrane with 0.3 µm pore size. Typically, membranes with micrometer-scale pore sizes exhibit lower LEP. Due to LEP limitations, we restricted our analysis to the experimental results obtained from membranes with nanometer-scale pore sizes. The influence of pore size on membrane performance is significant when subjected to applied hydraulic pressure. Smaller pore sizes allow membranes to withstand higher hydraulic pressures. Hence, we divided our findings into two sections based on the membrane pore sizes. Firstly, we demonstrated the performance of the TOEC process using a PTFE membrane with a 20 nm pore size and validated the model with experimental results. Then, we delved into the modeling results for PTFE membranes with pore sizes of 0.45 µm and 0.2 µm, as well as the PVDF membrane with a 0.3 µm pore size. We evaluated the impact of various factors on the performance of each membrane and conducted a comparative assessment to determine the optimal settings for the advancement of the TOEC process.

2.3.1 Performance evaluation of the PTFE membrane with 20 nm pore size and validation of the developed model

The viability of the TOEC process for real-world applications will be assessed by evaluating the performance of a PTFE membrane with a 20 nm pore size. The properties of this membrane are outlined in **Table 2.2** and were utilized in our simulations. As mentioned earlier, the key performance metrics for evaluating the TOEC process include vapor flux, TPC, thermal efficiency, energy efficiency, and power density. The operating conditions, such as feed temperature and applied hydraulic pressure, as well as the membrane properties, including porosity and thickness, are the most significant modeling inputs influencing the TOEC process. In this study, we will investigate how these modeling inputs affect the performance metrics of the process and identify the optimal conditions for effective operation.

Figure 2.4.A illustrates the effect of feed temperature on vapor flux and TPC of the system. The permeate temperature, applied pressure, and water flowrates were kept constant throughout this simulation at 20 °C, 10 bar, and 0.6 LPM, respectively. Increasing the feed temperature from 30 °C to 80 °C increased vapor flux from 1.46 LMH to 33.40 LMH, while the TPC decreased from 0.42 to 0.26. Due to the temperature polarization effect, the temperature of the membrane surface is always less than the bulk feed solution. When the feed bulk temperature increases, a thicker thermal boundary layer forms, leading to a more significant concentration polarization effect. Therefore, the temperature difference between the two sides of the membrane increases to a lesser extent than the bulk temperature difference. Consequently, the TPC of the system decreases, as indicated by Equation 2.16. The ideal feed temperature for achieving high vapor flux and TPC is the point of intersection between the two lines on the graph, which is found to be 64.3 °C.

Figure 2.4.B shows the impact of porosity on the thermal efficiency and TPC of the TOEC process. The modeling conditions for this graph remain the same as before, with the feed temperature fixed at 60 °C. As the porosity of the membrane increases from 60% to 90%, the thermal efficiency rises from 21.87% to 51.49%, and the TPC also increases from 0.33 to 0.36. Hence, to achieve high thermal efficiency and TPC in the TOEC process, it is necessary to increase the porosity of the membrane.

Membrane thickness is another crucial property that affects the TOEC process. The impact of membrane thickness on the energy efficiency and power density can be observed in **Figure 2.4.C**. As the membrane thickness increases from 50 μm to 250 μm, both energy efficiency and power

density decrease. Thicker membranes create a more substantial barrier for the vapor molecules to pass through the membrane.
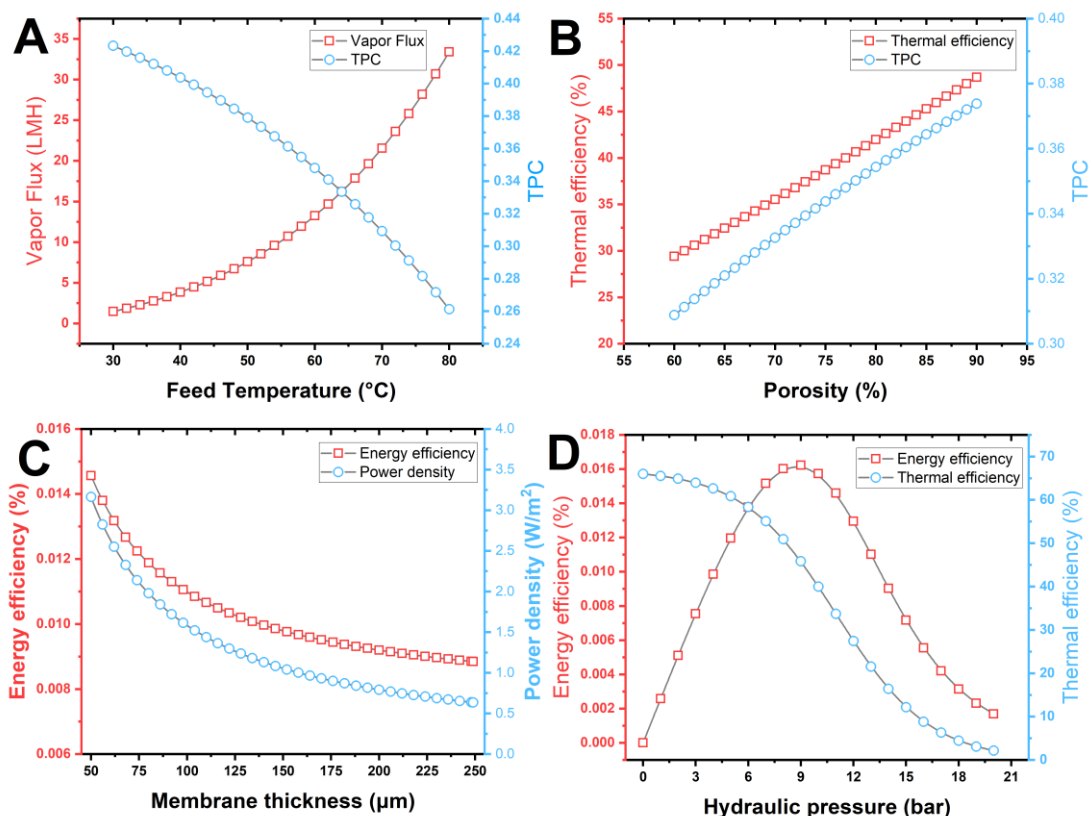
Figure 2.4. TOEC performance analysis for PTFE 20 nm pore size membrane. (A) effect of feed temperature on vapor flux and TPC of the system. (B) effect of porosity on thermal efficiency and TPC of the process. (C) effect of membrane thickness on energy efficiency and power density. (D) effect of applied pressure on energy efficiency and thermal efficiency.

One of the most critical factors affecting the TOEC process is the applied hydraulic pressure. By exerting pressure on the cold side of the membrane, we can depressurize the permeate stream and capture energy through the thermos-osmotic effect. To evaluate the impact of pressure on the TOEC process, we maintained the permeate and feed temperatures at 20°C and 60°C, respectively, while keeping the flowrates constant at 0.6 LPM on both sides. **Figure 2.4.D** illustrates the influence of hydraulic pressure on the system's thermal efficiency and energy efficiency. The thermal efficiency gradually declined as the pressure increased from 0 to 20 bar. However, the energy efficiency initially increased until a point where the reduction in vapor flux due to increased

pressure prevailed, resulting in decreased energy efficiency. The maximum energy efficiency observed was 0.016%, which occurred at a hydraulic pressure of 9.4 bar. Additionally, the graph demonstrates that if we desire both high energy and thermal efficiencies, an applied pressure of 6.3 bar should be employed.

Despite its currently low energy efficiency, the TOEC process offers a range of compelling commercial applications, primarily attributed to its innovative utilization of waste heat as a feed-side energy source, presenting an opportunity to recover energy that would otherwise dissipate. Moreover, TOEC holds promise for the desalination of seawater or brackish water, capitalizing on the osmotic gradient between solutions. TOEC's adaptability is further highlighted by its predicted role within integrated energy systems. These systems complement various renewable energy sources and energy conversion technologies, showcasing TOEC as a versatile component with a pivotal role in optimizing energy networks.

Figure 2.5.A depicts the impact of feed temperature and applied pressure on the power density of the TOEC process. Based on the graph, it can be concluded that the feed temperature should exceed 65 °C, while the pressure on the cold side needs to range between 6.2 bar and 11.8 bar to achieve power densities of > 5 W/m^2. The orange and red colors in the graph represent these optimal conditions.

The experimental data from the literature and our own results were used to validate the developed model for the PTFE 20 nm pore-size membrane [25]. The vapor flux was measured as a function of the applied hydraulic pressure. The membrane properties, operational settings, and simulation parameters were set to the conditions of the experiment. Straub et al. [25] achieved 24.6 LMH vapor flux under an applied pressure of 3.4 bar, followed by fluxes of 18.8 LMH at 6.9 bar pressure, 13.5 LMH at 10.3 bar pressure, and 2.3 LMH at 13.8 bar pressure. As can be seen in **Figure 2.5.B**, a good agreement between the developed model and the experimental results was observed. Increasing the applied pressure resulted in a decrease in vapor flux due to the elevated vapor pressure on the cold side caused by higher pressure. Additionally, higher applied pressure led to more significant membrane compaction, thereby reducing the membrane's vapor permeability. Consequently, the diminished vapor permeability at higher pressures further contributed to the decline in vapor flux.
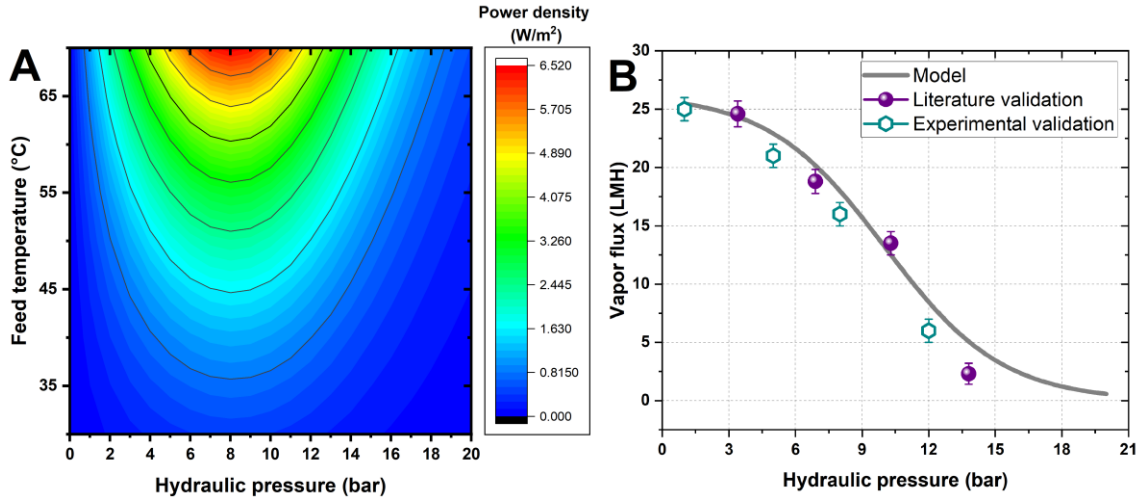
Figure 2.5. (A) Effect of feed temperature and applied pressure on the power density of the system. (B) Validation of the developed model for a PTFE 20 nm pore-size membrane. The effect of applied pressure on the vapor flux is depicted for both modeling and experimental results. Some experimental data were obtained from [4].

2.3.2 Modeling results on micrometer scale pore size membranes

2.3.2.1 Effect of feed temperature

One of the key factors that significantly affect the overall performance of the TOEC system is the feed temperature. **Figure 2.6.A–C** illustrates the impact of feed temperature on important performance metrics, namely TPC, thermal efficiency, and power density. We maintained the permeate temperature at 20 °C, the feed and permeate flowrates at 0.6 LPM, and the applied hydraulic pressure at 10 bar. As depicted in **Figure 2.6.A**, the TPC of the system for all three membranes will decrease as the feed temperature increases from 30 °C to 90 °C. This trend can be attributed to the thermal resistance created by a thicker thermal boundary layer adjacent to the feed side of the membrane at higher temperatures. Increasing the feed water temperature results in a larger bulk temperature difference compared to the surface temperature difference. Consequently, the TPC, which represents the ratio of surface temperature difference to the bulk temperature difference, decreases with an increase in the feed temperature. A higher TPC indicates that the transmembrane temperature difference is closer to the bulk temperature difference on both sides of the membrane. However, TPC alone is insufficient for determining the optimal condition of a TOEC process. When the feed temperature increases, both vapor flux (J_w) and $T_{H,m} - T_{C,m}$ in Equation 19 increase. The interplay between these parameters influences the thermal efficiency trend. According to **Figure 2.6.B**, when the feed temperature is increased, the enhancement of

37

water flux has a more pronounced effect on thermal efficiency compared to the increase in surface temperature difference. As an illustration, when examining PTFE with a pore size of 0.45 μm, the vapor flux substantially increased from 2.01 to 43.02 LMH as the feed temperature escalated from 30 to 90 °C.

Furthermore, among the three membranes studied, the PVDF membrane with a pore size of 0.3 μm exhibits the highest TPC, while the PTFE membrane with a pore size of 0.45 μm demonstrates the lowest TPC. This distinction arises from the different thermal conductivities of PTFE and PVDF membranes (0.2726 W/mK for PTFE compared to 0.1926 W/mK for PVDF). Additionally, as shown in **Table 2.2**, the PTFE membrane is thinner than PVDF. As a result, based on Fourier's law of thermal conduction, PTFE allows for more heat conduction through the membrane, increasing the temperature of the membrane surface on the permeate side. Therefore, the transmembrane temperature difference experienced by the PTFE membrane is lower than that of the PVDF membrane, which results in a lower TPC for PTFE. Nevertheless, the 0.45 μm PTFE membrane shows better thermal efficiency due to the high vapor flux through this membrane.

The effect of feed temperature on thermal efficiency and power density is illustrated in **Figure 2.6.B and C**, respectively. Since the driving force for vapor flow across the membrane is the vapor pressure difference, increasing the feed temperature leads to an increase in the vapor pressure difference and the driving force for vapor to flow across the membrane. This increased vapor flow subsequently results in greater liquid flow via the hydro turbine, leading to higher output power. As mentioned above, according to Equation 2.19, a higher feed temperature increases permeate flow, ultimately resulting in higher thermal efficiency. Therefore, Increasing the feed temperature increases the system's thermal efficiency and power density. The PTFE membrane with a pore size of 0.45 μm demonstrates the highest thermal efficiency and power density, while the PVDF membrane exhibits the lowest power density. Additionally, the PTFE membrane with a pore size of 0.2 μm exhibits the lowest thermal efficiency among the three membranes compared. The higher vapor flux and power density of PTFE membranes can be attributed to their lower thickness and higher hydrophobicity when compared to the PVDF membrane. Furthermore, the PTFE membranes, with larger pore size in the case of 0.45 μm compared to 0.2 μm, exhibit higher vapor flux and power density. Moreover, due to their larger thermal conductivity and lower thickness, the PTFE membranes offer superior heat conduction compared to the PVDF membrane. Hence,

the thermal efficiency competition among the three membranes relies on the intricate balance between heat conduction and heat convection, which is governed by vapor flux.
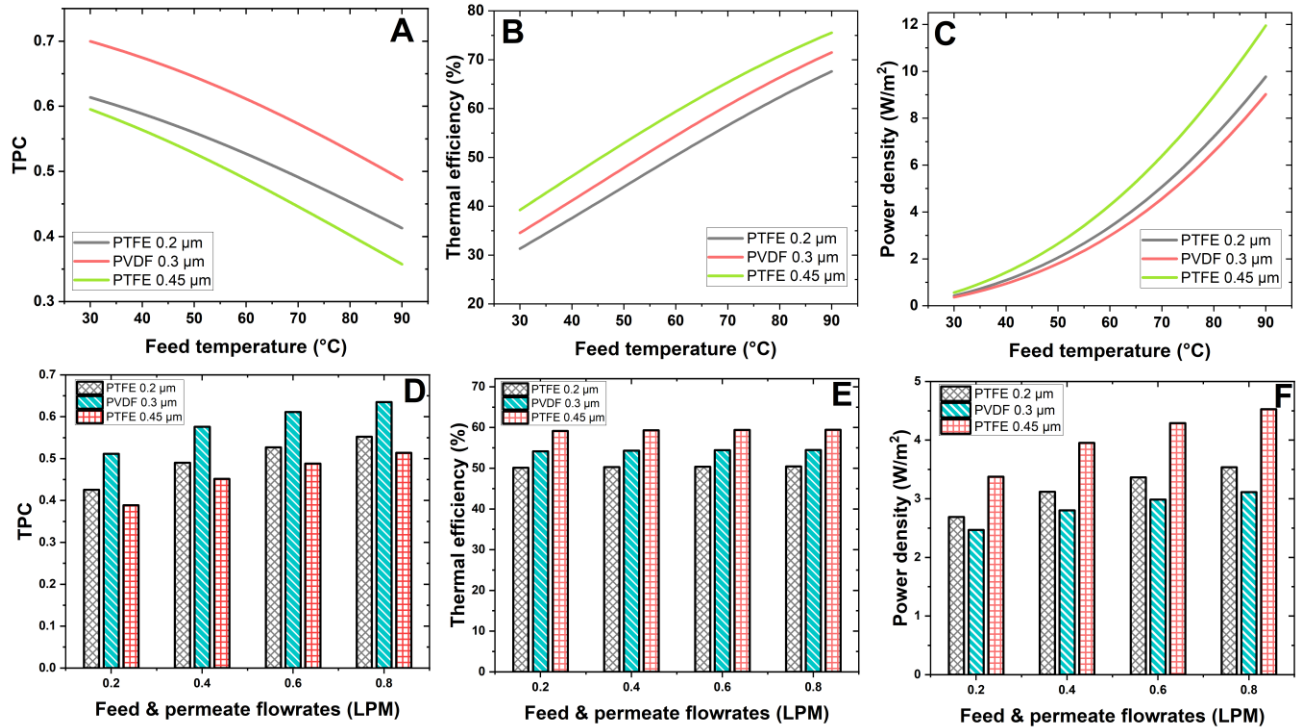
Figure 2.6. TOEC performance based on different feed temperatures and flowrates for PTFE 0.45, PTFE 0.2, and PVDF 0.3 μm pore size. Effect of temperature on (A) TPC, (B) thermal efficiency, and (C) power density, and effect of feed and permeate flowrates on (D) TPC, (E) thermal efficiency, and (F) power density.

2.3.2.2 Effect of feed and permeate flowrates

To assess the impact of the feed and permeate flowrates on the simulation results, we maintained the feed and permeate temperatures at 60 and 20 °C, respectively, and the applied hydraulic pressure at 10 bar. **Figure 2.6.D-F** depicts the impact of feed and permeate flowrates on the performance of a TOEC process. With an increase in flowrates, the vapor flow across the membrane also escalates. This can be attributed to enhanced mixing and faster diffusion of vapor molecules. The enhanced mixing facilitates more efficient interaction between the vapor molecules and the membrane surface. Consequently, vapor molecules can diffuse more rapidly through the membrane, increasing vapor flux. Given that, the TPC and power density of the system increase as the flowrates rise from 0.2 LPM to 0.8 LPM, while the thermal efficiency remains relatively constant. According to Equation 2.16, TPC represents the temperature difference at the membrane surface relative to the bulk temperature difference. An increase in TPC indicates an amplified

surface temperature difference, leading to a greater driving force for vapor flow and increased vapor flux. Consequently, the power density also increases. However, in the range of investigated flowrates, the interplay between surface temperature difference and vapor flux (Equation 2.19) imposed a negligible effect on thermal efficiency.

2.3.2.3 Effect of membrane thickness

One of the crucial membrane characteristics that significantly affect TOEC performance is membrane thickness. This section investigates the impact of membrane thickness on TOEC performance. To assess this impact, we maintained the feed and permeate temperatures at 60 and 20 °C, respectively, while fixing the feed and permeate flowrates at 0.6 LPM, and the applied hydraulic pressure at 10 bar. As shown in **Figure 2.7.A**, the vapor flux drops as the membrane thickness increases from 50 to 600 μm because a thicker membrane acts as a stronger barrier for vapor passage through the membrane. Consequently, the power density of the process decreases as lower vapor flow corresponds to lower power density (**Figure 2.7.B**). For instance, in the case of PTFE 0.45 μm pore size, increasing the membrane thickness from 50 to 600 μm leads to a decrease in power density from 5.62 to 1.31 W/m². Similarly, for PTFE 0.2 μm and PVDF 0.3 μm pore sizes, the power density decreases from 4.52 to 0.97 W/m² and from 4.95 to 1.09 W/m², respectively.

As demonstrated in **Figure 2.7.C**, the energy efficiency of the system improves slightly as the membrane thickness increases, implying the dominant effect of improved conduction resistance (to maintain a high surface temperature difference) as compared to increased vapor flux. It can also be inferred that, under the same conditions and properties, the PTFE 0.45 μm membrane exhibits higher vapor flux, energy efficiency, and power density than the PVDF membrane. Similarly, the PVDF membrane outperforms the PTFE 0.2 μm pore size membrane in terms of the aforementioned performance metrics. The larger pores in the membrane result in increased vapor flow, improving both power density and energy efficiency.

2.3.2.4 Effect of applied hydraulic pressure

The main distinction between MD and the TOEC process lies in the applied hydraulic pressure on the permeate side of the membrane, specifically employed in TOEC to utilize the thermos-osmotic energy generated by the temperature gradient. However, applying pressure can pose significant challenges to the energy output of the TOEC process, as membranes may not function optimally

under pressure. Therefore, it is crucial to assess the impact of applied pressure on the performance of the TOEC process. This section investigates the effect of applied pressure on vapor flux, energy efficiency, and power density, with the applied pressure varying between 1 and 30 bar. The feed and permeate flowrates were maintained at 0.6 LPM, while the feed and permeate temperatures were fixed at 60 and 20 °C, respectively. As illustrated in **Figure 2.7.D**, vapor flux decreases with increasing applied pressure, which aligns with theoretical expectations. The vapor pressure on the cold side diminishes as the applied pressure rises, and membrane compaction can significantly impair the membrane's performance by impeding vapor passage through the membrane pores. Consequently, increasing the applied pressure leads to a reduction in vapor flux. The effect of applied pressure on power density and energy efficiency is depicted in **Figure 2.7.E and Figure 2.7.F**, respectively. The power density initially increases as the pressure increases from 1 to 30 bar. However, at a certain point (between 10-15 bar), the power density starts to decline with further increases in applied pressure. Since power density is determined by multiplying the applied hydraulic pressure by the vapor flux [13], it initially increases as the applied pressure grows. However, when the applied pressure reaches a level where the reduction in vapor flux outweighs the impact of increased pressure, the power density of the system decreases. Similar reasoning applies to the effect of applied pressure on energy efficiency, as shown in **Figure 2.7.F**. Since energy efficiency is calculated as the ratio of work output to thermal energy input [11], the same trend can be observed. According to these findings, the applied pressure to the cold side of different micrometer pore size membranes should be adjusted between 10 and 15 bar to get the highest power density and energy efficiency in a TOEC process. Furthermore, the optimal hydraulic pressure that yields the highest power density varies among different membrane types. It is 11.2 bar for PVDF with a 0.3 µm pore size, 11.4 bar for PTFE with a 0.2 µm pore size, and 11.9 bar for PTFE with a 0.45 µm pore size. The corresponding maximum power density values for these membranes are 3.02 W/m², 3.42 W/m², and 4.41 W/m², respectively. Similarly, to achieve the highest energy efficiency, the optimal hydraulic pressures are 13.5, 14, and 14.5 bar for 0.2 µm PTFE, 0.3 µm PVDF, and 0.45 µm PTFE, respectively. Notably, in the pursuit of maximizing both power density and energy efficiency, the optimal hydraulic pressure for PTFE with a pore size of 0.45 µm surpasses that of the other two membranes. This deviation in optimal hydraulic pressure can be attributed to the unique structural characteristics and permeability of each membrane. The

PTFE 0.45 μm pore size likely requires a higher hydraulic pressure to effectively balance the high fluid flow within its pores.
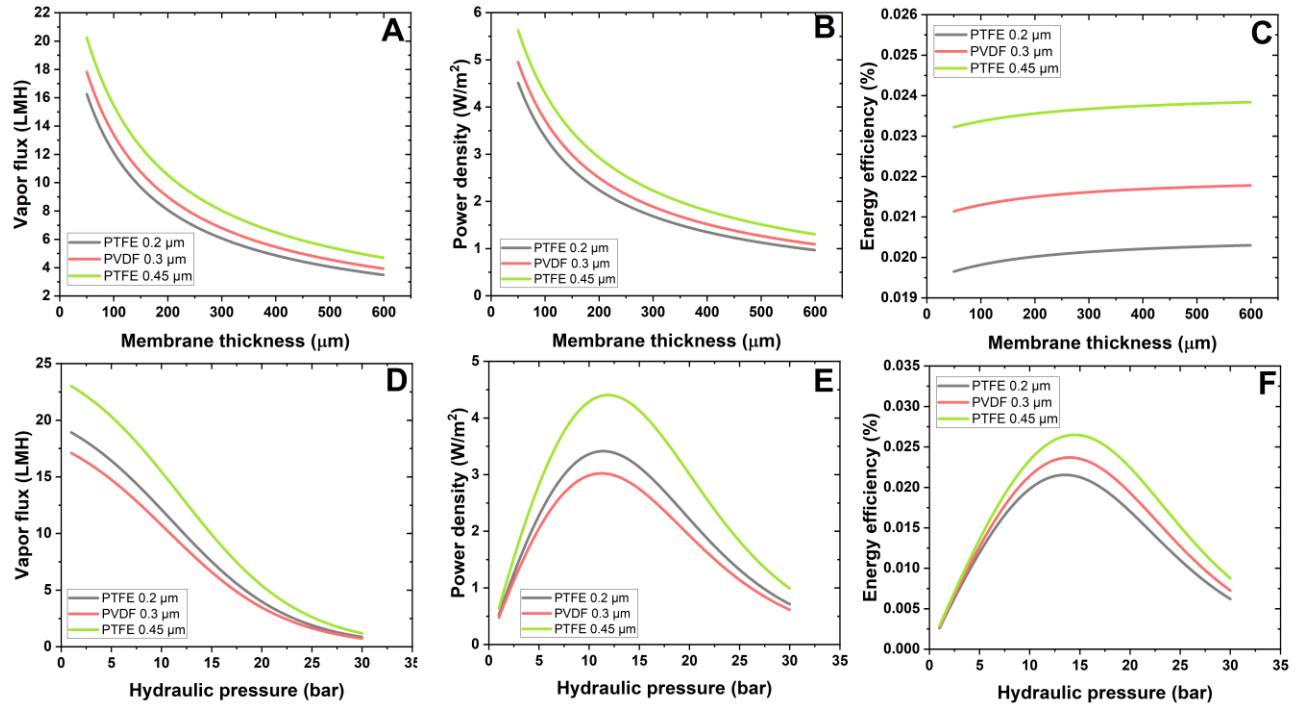
Figure 2.7. Performance evaluation of a TOEC system based on membrane thickness and hydraulic pressure for micrometer pore size membranes (PTFE 0.45, PTFE 0.2, and PVDF 0.3 μm pore size). Effect of membrane thickness on (A) vapor flux, (B) power density, and (C) energy efficiency. Effect of hydraulic pressure (D) vapor flux, (E) power density, and (F) energy efficiency.

2.4 Conclusion

In this study, a comprehensive mathematical model based on ∈-NTU method was developed to evaluate the feasibility of a TOEC system under various system conditions. Factors such as feed temperature, feed and permeate flowrates, membrane thickness, membrane porosity, and applied hydraulic pressure were considered. By appropriately adjusting the operating conditions (temperature, flowrates, applied pressure) and membrane properties (pore size, porosity, thickness), the TOEC system can achieve optimal performance. The developed model enables the prediction of vapor flux, temperature polarization, thermal efficiency, energy efficiency, and power density of the TOEC system. This investigation examined different membranes with varying characteristics, initially focusing on three membranes with large pore sizes (PTFE 0.45

μm, PTFE 0.2 μm, and PVDF 0.3 μm pore size). For all three membranes, increasing the feed temperature, flowrates, and membrane porosity enhanced vapor flux. In contrast, reducing the membrane thickness and hydraulic pressure improved vapor flux across the TOEC membrane. Except for hydraulic pressure, it was recommended to increase the other modeling inputs to achieve high thermal efficiency and energy efficiency. To further enhance thermal efficiency, minimizing the hydraulic pressure was suggested, with a range of 10 to 15 bar being potentially suitable for maximizing energy efficiency. Furthermore, lowering the feed temperature and membrane porosity while increasing the flowrates, membrane thickness, and applied pressure was found to raise the system's TPC. Power density, one of the most crucial performance indicators, increased by increasing feed temperature, flowrates, and membrane porosity but decreased by increasing the membrane thickness.

Due to the large pore diameters of the examined membranes, their Liquid Entry Pressure (LEP) was extremely low, and membrane pore wetting could occur even at such low pressures. To assess the effectiveness of the TOEC system under higher applied pressures, a membrane with nanometer-sized pores (PTFE with a 20 nm pore size) was used. The modeling results for this particular membrane revealed that an optimal feed temperature of 65 °C is ideal for achieving high TPC and vapor flow. The impact of membrane properties, such as porosity and thickness, was also examined. Increasing the membrane's porosity improved the TPC and thermal efficiency of the system while increasing the membrane's thickness had the opposite effect. At a pressure of 9.4 bar, the highest energy efficiency achievable with this membrane was 0.016%. It was also concluded that the applied pressure should be 6.3 bar to achieve high thermal and energy efficiency. The feed temperature needed to be above 65 °C, and the pressure on the cold side should be in the range of 6.2 to 11.8 bar to achieve a higher power density than 5 W/m2 for the TOEC process. The provided design map offers valuable guidance to researchers for appropriately adjusting the operating conditions and utilizing optimal membrane properties. The modeling results were found to be in excellent agreement with experimental results from this study and the literature. In order to advance the implementation of the TOEC process on a larger scale, it is imperative to conduct further research aimed at fabricating specialty TOEC membranes that possess enhanced LEP and mechanical strength.

3 Life-Cycle Assessment of Membrane Synthesis for the Application of TOEC Process

3.1 Introduction

In a world with growing energy demands and increasing concerns about climate change, it is essential to use available energy resources wisely. At the heart of this challenge lies the need to efficiently capture low-grade waste heat—an abundant and frequently overlooked energy source found in industrial processes, power generation, and numerous other applications [6,111–113]. The quest to convert this otherwise wasted energy into a valuable resource has driven innovation and led to the emergence of novel technologies. Among these, the Thermo-Osmotic Energy Conversion (TOEC) process stands as a promising avenue for transforming low-grade waste heat into usable power [25,69,114]. This innovative technology harnesses temperature gradients to induce a partial vapor pressure across a hydrophobic membrane. This pressure differential propels vapor from the hot feed side, through the membrane's pores, to the cold permeate side. The resulting movement of water from the hot feed side to the permeate side induces an accumulation of excess fluid in the cold reservoir, ultimately generating a pressurized flow that can be effectively utilized to drive a turbine, thus producing electricity [11,114].

While TOEC shows remarkable promise for converting low-grade heat into electricity, the widespread implementation of this technology is not without its challenges. At the heart of these challenges lies the critical role of membranes in the TOEC process [11,66]. One crucial component of the TOEC process is the membrane used to facilitate osmotic transport [65,100]. The choice of membrane material is pivotal in determining the efficiency, durability, and environmental impact of the entire TOEC system. Two common membrane materials used in the TOEC process are Polyvinylidene Fluoride (PVDF) and Polytetrafluoroethylene (PTFE). These membranes possess distinct characteristics that directly influence the performance and feasibility of TOEC technology. PVDF is a widely adopted membrane material known for its robustness and chemical resistance

[115–117]. PVDF membranes exhibit a remarkable tolerance to harsh operating conditions, making them suitable for a range of applications [116,118]. PTFE is another commonly employed membrane material with its own set of advantageous properties. PTFE membranes are renowned for their exceptional hydrophobicity, which minimizes the unwanted intrusion of liquid water into the membrane structure [119,120]. The selection of the appropriate membrane material, whether PVDF or PTFE, is a crucial decision in TOEC system design.

However, a thorough life-cycle analysis is imperative to ensure the careful and informed adoption of these membranes. Currently, there is a lack of systematic assessment regarding the environmental impacts of PTFE and PVDF membrane synthesis. This knowledge gap could potentially hinder the integration of environmentally friendly practices into the industrialization of the TOEC process, leading to missed opportunities for sustainable energy generation. It is essential to assess the cumulative energy demand (CED) and environmental impacts of lab-scale synthesis of these membranes through a Life Cycle Assessment (LCA) approach.

LCA provides a holistic framework for evaluating the energy demand and the environmental implications of a product or process throughout its entire life cycle [73,74,121,122]. Data collection and inventory analysis are conducted to gather information on the energy and material inputs, emissions, and other relevant environmental aspects associated with membrane synthesis. This includes assessing the raw material extraction, manufacturing processes, energy consumption, and waste generation [74,76]. We curated the inventory data from our lab data and various published studies on laboratory-scale PTFE and PVDF membrane syntheses.

Once the inventory data is collected, impact assessment methods are used to evaluate the environmental impacts associated with membrane synthesis. These methods help quantify the potential effects on various environmental categories, such as climate change, human health, ecosystems, and resource depletion. By examining these impacts, LCA provides a comprehensive overview of the environmental performance of PTFE and PVDF membranes for TOEC. The results of the LCA can then be used to guide decision-making processes, such as selecting optimal membrane materials, identifying opportunities for process optimization, or comparing different membrane synthesis approaches.

45

In this groundbreaking study, we comprehensively assessed the cumulative energy demand and environmental impacts related to the synthesis of PTFE and PVDF membranes. This pioneering work represents the first-ever life cycle assessment that covers both laboratory-scale synthesis and large-scale production of these crucial membranes utilized in the TOEC process. By meticulously analyzing the entire life cycle, from raw material extraction to end-of-life stages, we gained valuable insights into the total energy requirements and environmental implications of producing PTFE and PVDF membranes. Our study fills a significant knowledge gap and lays the foundation for understanding the sustainability and energy demand aspects of these membranes in the context of TOEC. The findings offer essential guidance for decision-makers, allowing them to make informed choices regarding optimal membrane materials and processes, promoting sustainable practices, and exploring environmentally friendly alternatives.

3.2 Material and Methods

PTFE and PVDF membranes can be fabricated via different routes. It should be noted that during the fabrication process of membranes, the electrical devices' power usage is carefully managed. Specifically, the stirrer, muffle furnace, and oven were considered to operate at power levels of 50 W, 1000 W, and 800 W, respectively.

The PTFE membrane was prepared using the paste extrusion-stretching method, following a step-by-step procedure. Initially, aqueous polyvinyl alcohol (PVA) solution was meticulously prepared by dissolving PVA powder in distilled water at 90 ºC while ensuring constant agitation for a minimum of 6 hours. A lubricant is added to the PTFE resin to facilitate the extrusion process. The lubricant helps to reduce friction and improve the flow properties of the PTFE resin. The most commonly used lubricant for PTFE membrane fabrication is naphtha. Subsequently, a predetermined amount of aqueous PTFE dispersion was added to the PVA solution, maintaining a PTFE-PVA mass ratio of 4:1. Non-ionic surfactants are commonly used to stabilize the PTFE emulsion and prevent coagulation of the particles. During the preparation of the PTFE emulsion, the surfactant is added to ensure proper emulsification. The addition of non-ionic surfactants during PTFE membrane fabrication can help control the pore size and morphology of the membrane. The resulting solution, which appeared heterogeneous, was gradually cooled to room

temperature. After 3 hours of continuous stirring, the solution underwent a degassing process under vacuum for 8 hours. Next, the solution was cast onto a clean and smooth stainless-steel plate to form films, which were further immersed in pure ethanol to yield PTFE-PVA composite films. These films were air-dried and subsequently sintered in a muffle furnace at 360 $^{\circ}$C for 3 minutes. Upon cooling, the sintering process caused the PVA matrix to decompose, resulting in the fusion of the remaining PTFE resins to form an interconnected continuous structure, thus producing the PTFE membranes. To conduct a detailed analysis of PTFE membrane fabrication on a small scale, we employed the following precise formulation: 60 grams of PTFE, 15 grams of PVA, 5 grams of naphtha, 45 grams of deionized water, 5 grams of a non-ionic surfactant, and 10 grams of ethanol. This meticulous combination yielded a PTFE membrane with a surface area of 1430 cm^2.

The PVDF membrane was prepared using the phase inversion process, following a detailed procedure. Initially, the dope solution was created by blending LiCl (5 wt.%) to enhance the coagulation rate, SiO$_2$ (2 wt.%) as well as Dimethylacetamide (DMAc) (81%) as the solvent. PVDF (12 wt.%) was then introduced into the dope solution and stirred at 300 rpm at 60 °C for 24 hours, ensuring complete dissolution and homogeneous solution. Modified SiO$_2$ nanoparticles were incorporated into the PVDF precursor solution to increase surface roughness. Research studies have shown that adding hydrophobic SiO2 increases porosity, resulting in an elevated permeate flux. The polymer solution was subsequently degassed in a vacuum oven at room temperature for 4 hours. The dry-wet phase inversion process was employed to manufacture the flat sheet membrane. Initially, a piece of polyester support was affixed to a glass plate. The polymer solution was then cast onto a nonwoven fabric using a 0.15-micrometer casting knife. After being exposed to air for 15 seconds, the film was immersed in a DI water bath at 25 °C, allowing for phase inversion to occur. Once the phase inversion was complete, the solidified polymer sheet was carefully detached from the plate and soaked in deionized water at ambient temperature for 24 hours. Subsequently, it was soaked in ethanol and n-hexane for 15 minutes each to minimize shrinkage effects by gradually reducing surface tension during drying. Finally, the membrane was dried for 24 hours at room temperature. To fabricate a 280 cm^2 PVDF membrane for our small-scale analysis, we considered the combination of the following materials: 2.4 grams of PVDF, 16.2 grams of DMAc, a 320 cm^2 polyester substrate, 100 grams of DI water, 1 gram of LiCl, 0.4 grams of SiO$_2$, 1.5 grams of ethanol, and 1.5 grams of n-hexane.

3.3 Results and Discussion

We conducted a comprehensive LCA analysis of PVDF and PTFE membrane fabrication, considering both small-scale and large-scale production.

3.3.1 Small scale assessment

We considered lab-scale fabrication of 1430 cm2 and 280 cm2 for the small-scale assessment for PTFE and PVDF membranes, respectively. In this evaluation, we carefully analyzed the cumulative energy demand and environmental implications associated with manufacturing these membranes.

3.3.1.1 Cumulative energy demand (CED) of PTFE and PVDF membrane synthesis

The CED values represent the total energy consumption included throughout the entire production lifecycle of a product. CED considers energy from various sources, including both non-renewable (e.g., fossil fuels) and renewable (e.g., solar, wind, hydro) sources [74,123]. Lower CED values indicate that the production process is more energy-efficient, resulting in reduced resource consumption [124]. **Figure 3.1.** shows the CED values attributed to the manufacturing process of two distinct types of membranes, namely PTFE and PVDF. As evident from the data, the production of 1430 cm^2 of PTFE membrane entails the energy consumption of 8.187 MJ from fossil sources, 6.348 MJ from renewable biomass sources, 1.598 MJ from nuclear sources, 0.624 MJ from water sources, 0.349 MJ from non-renewable biomass sources, and 0.282 MJ from wind, solar, and geothermal sources across the membrane's entire lifecycle. Conversely, in the case of the 280 cm^2 of PVDF membrane production, the energy consumption comprises 3.578 MJ from fossil sources, 2.802 MJ from renewable biomass sources, 0.268 MJ from nuclear sources, 0.12 MJ from water sources, 0.041 MJ from non-renewable biomass sources, and 0.06 MJ from wind, solar, and geothermal sources throughout the membrane's lifecycle. These findings clearly demonstrate the significant influence of fossil and renewable biomass energy sources. Fossil sources contribute to 47.1% of PTFE membrane's total CED and 52.1% of PVDF membrane's total CED, while renewable biomass sources account for 36.5% of PTFE membrane's total CED and 40.8% of PVDF membrane's total CED. In both cases, fossil fuel and renewable biomass sources stand out as the primary contributors to the CED, while other energy sources, such as non-renewable biomass, nuclear, water, wind, solar, and geothermal, have a negligible impact on the

48

CED of both membranes. This dependence on fossil sources is a matter of concern from both environmental and resource availability perspectives.

Fossil-based energy is finite and contributes significantly to greenhouse gas emissions [125,126]. The high proportion of fossil fuel energy in the CED of these membranes suggests a considerable carbon footprint associated with their production. Moreover, the finite nature of fossil fuels raises questions about the long-term sustainability of these materials if their production continues to rely heavily on such energy sources. This aspect underscores the urgency of exploring alternative, more sustainable energy options for membrane production, such as greater integration of renewable energy sources like wind, solar, and geothermal, which currently comprise only a minor fraction of the CED. Conversely, the relatively lower CED attributed to renewable biomass sources in manufacturing both PTFE and PVDF membranes is a noteworthy consideration. Renewable biomass sources account for 36.5% of the CED for PTFE and 40.8% for PVDF. This indicates that these materials have made efforts to incorporate more sustainable energy sources in their production processes. While renewable biomass sources are certainly more sustainable than fossil fuels, it is essential to ensure that the biomass used is produced in an environmentally responsible and sustainable manner. The choice of biomass sources and their management can significantly impact the overall environmental sustainability of these membranes.
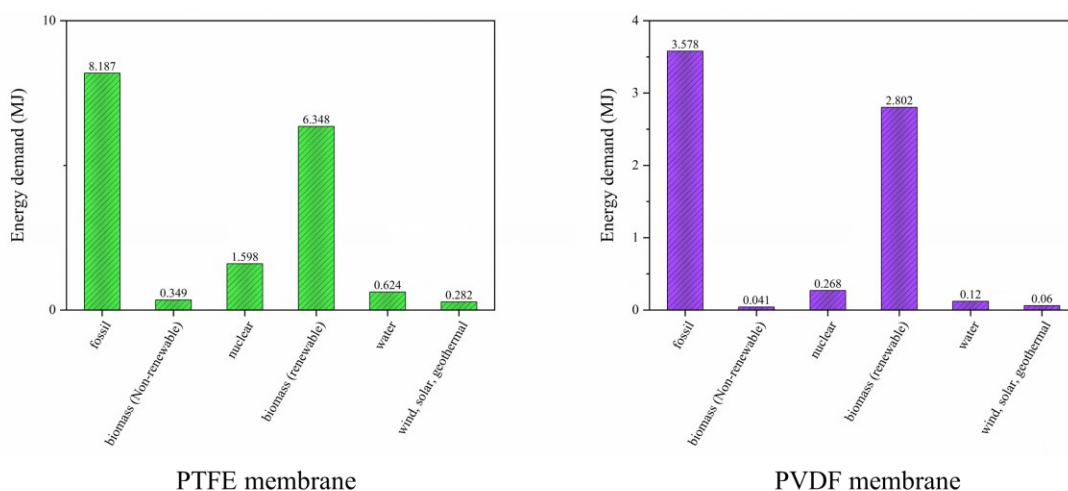

Figure 3.1. Cumulative energy demand associated with the lab-scale production of PTFE and PVDF membrane. In the small-scale evaluation, we considered the fabrication of 1430 cm^2 of PTFE membrane and 280 cm^2 of PVDF membrane.

Figure 3.2. illustrates the chemical contributions to the CED of the PTFE membrane for various energy sources and provides deeper insights into the specific factors affecting the overall energy demand of this membrane's production. These insights offer a crucial avenue for optimizing the manufacturing process and making it more environmentally sustainable. Notably, PTFE resin exhibits the most significant impact on the fossil-based CED, accounting for 44.5% of the total fossil CED. In contrast, for non-renewable biomass sources, polyvinyl alcohol emerges as the primary contributor, contributing to 89.5% of the CED derived from non-renewable biomass sources. Regarding nuclear energy sources, PTFE resin dominates, contributing to 71.2% of the corresponding CED. In the context of renewable biomass, nonionic surfactants dominate, being responsible for 61.9% of the CED. It indicates that this specific chemical plays a crucial role in the energy-intensive processes related to the use of renewable biomass sources. In the case of water energy sources, PTFE resin plays a crucial role, contributing to 67.6% of the CED. As for wind, solar, and geothermal sources, the contributions of PTFE resin and electricity are higher than the rest of the chemicals, amounting to 48.9% and 28.9%, respectively. Overall, these results highlight the varying degrees of chemical impact on the CED for different energy sources, with PTFE resin often being the primary contributor. Given that PTFE resin is an indispensable component for fabricating PTFE membranes and cannot be substituted with another chemical, it is recommended that alternatives for the chemicals with significant energy demands be explored. This approach can help reduce the CED associated with the production process. For instance, to address the energy demand concern associated with renewable biomass sources, exploring alternative options to replace nonionic surfactants in the production of PTFE membranes is imperative.

Figure 3.2. Contribution of each chemical to the energy demand of PTFE membrane synthesis for various energy sources.

Figure 3.3. illustrates the contribution of each chemical to the CED of the PVDF membrane. One striking observation is the dominance of ethanol as the primary contributor to the CED for both renewable and non-renewable energy sources, accounting for 65.5% and 70%, respectively. This prominence can be attributed to ethanol being commonly derived from biomass sources [127]. DMAc and electricity have the highest contributions (43.9% and 27.5%, respectively) to the CED of membrane synthesis for fossil-based energy sources. PVDF powder and DMAc play pivotal roles in the CED of nuclear-based energy sources, contributing 40.5% and 34.5%, respectively. Most chemicals make comparable contributions to water-based energy sources, but DMAc, electricity, and PVDF powder are the dominant contributors to the CED. In the context of wind, solar, and geothermal energy sources, electricity emerges as the primary contributor, making up 54.7% of the CED of the membrane synthesis. In summary, these findings underscore the substantial impact of DMAc, electricity, and ethanol on the CED of the PVDF membrane, with

different chemicals assuming varying degrees of importance depending on the energy source used in the synthesis. Therefore, it is important to find alternatives for the chemicals that are dominant contributors to decrease the CED of PVDF membrane synthesis. It is important to explore alternative solvents or methodologies that reduce the reliance on DMAc, which is a chemical with a significant energy footprint. Developing more energy-efficient methods of electricity generation and utilization in the synthesis process is also crucial to decreasing the energy demand associated with PVDF membrane production.

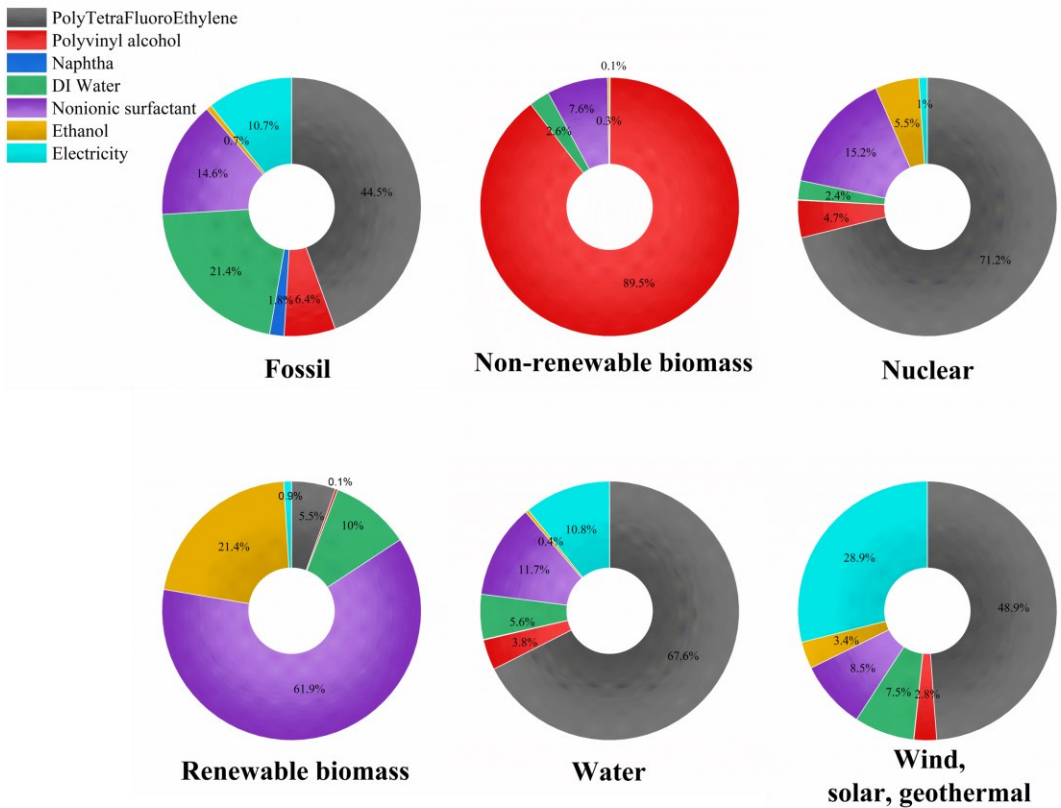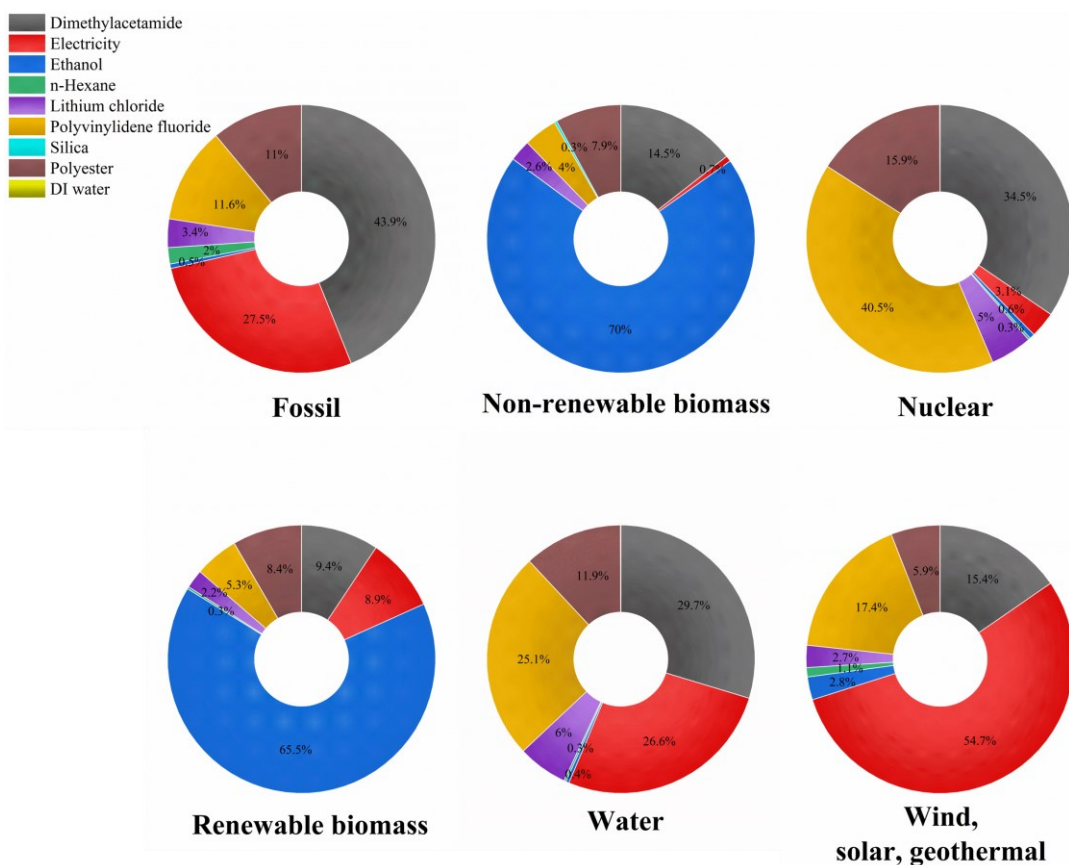**Figure 3.3.** Contribution of each chemical to the energy demand of PVDF membrane synthesis for various energy sources.

By presenting these CED values, researchers and industry stakeholders gain valuable insights into the energy demand throughout the entire lifecycle of PTFE and PVDF membrane production. This information can aid in making informed decisions regarding material selection, process optimization, and the pursuit of more eco-friendly alternatives.

3.3.1.2 Environmental impacts of PTFE and PVDF membrane synthesis

LCA has significant implications for evaluating the environmental impacts associated with the synthesis of PTFE and PVDF membranes. This chapter aims to assess the environmental impacts of lab-scale synthesis for both types of membranes, considering resource utilization, chemical emissions, and stressor potency, utilizing the underlying techniques in TRACI. The models and data employed for each impact category ensure accuracy in evaluating potency. For certain impact categories, such as ozone depletion and global warming effects, there exists an international agreement on the relative potency of the chemicals listed. However, for other impact categories, relative potency is determined based on chemical and physical principles or experimental data models [74]. The following environmental impact categories are defined and described in detail [74,128–131]:

Acidification: It refers to the process of a local environment becoming more saturated with hydrogen ions (H^+). This can result from the introduction of acids (e.g., nitric and sulfuric acid) or other substances (like ammonia) that increase environmental acidity through various chemical reactions and/or biological activities. It can also be caused by natural events, such as changes in soil concentrations due to the expansion of local plant species.

Eutrophication: It occurs when aquatic habitats are enriched with nutrients (e.g., nitrates and phosphates), leading to increased biological productivity, such as the growth of algae and weeds. This results in an undesirable accumulation of algal biomass.

Global Warming: It refers to the average rise in temperature of the Earth's atmosphere near the surface and in the troposphere. It can lead to changes in the planet's climate patterns. Global warming can be caused by both natural factors and human activities, with elevated greenhouse gas emissions from human activities being a significant contributor.

Ozone Depletion: It refers to the reduction of ozone in the stratosphere, which can lead to increased radiation reaching the Earth's surface. This, in turn, can have adverse effects on human health, including an increased risk of skin cancer and cataracts. Ozone depletion also impacts human-made objects, marine life, and other plants and animals. Certain substances, such as chlorofluorocarbons and halons, have been linked to lowering stratospheric ozone levels. Efforts to reduce these substances have been made through international agreements like the Montreal Protocol.

Respiratory Effects: In this category, the focus is on particulate matter and its precursors. Particulate matter consists of microscopic airborne particles that can adversely affect human health, particularly respiratory health. Elevated levels of ambient particulate matter have been associated with increased mortality risk, particularly from respiratory diseases. Precursors to secondary particulates include nitrogen oxides and sulfur dioxide (NO_x and SO_2), which are frequently produced by burning fossil fuels, wood, and dust from fields and highways.

Carcinogenic, Non-carcinogenic, and Ecotoxicity: A carcinogen is any agent, substance, radionuclide, or form of radiation that promotes the onset and progression of cancer. Ecotoxicity refers to the effects of toxic substances on various environments, such as urban and non-urban air, freshwater, seawater, natural soil, and agricultural soil. In LCA, the Comparative Toxic Unit for Humans (CTUh) and Comparative Toxic Unit for Ecosystem (CTUe) are used as indicators for carcinogenic and ecotoxic impacts, respectively.

Smog: Smog is a severe form of air pollution resulting from chemical reactions between sunlight, volatile organic compounds, and nitrogen oxides. Ground-level ozone, a component of smog, can cause respiratory problems and permanent lung damage in humans. Smog can also harm crops and ecosystems.

Figure 3.4. illustrates the environmental impacts of PTFE membrane synthesis, and the contribution of each chemical to impact categories is demonstrated. These findings not only pinpoint the primary contributors to various environmental impact categories but also offer valuable guidance on how to mitigate these impacts and foster more sustainable manufacturing practices. In all impact categories, except for eutrophication, PTFE resin emerges as the primary contributor among all chemicals. In the case of eutrophication, electricity takes the lead, while PTFE resin follows as the second-highest contributor. Overall, it is evident that PTFE resin, electricity, and nonionic surfactants dominate the majority of environmental impact categories. As a result, it is advisable to consider substituting nonionic surfactants with greener alternatives in the PTFE membrane fabrication process and reducing electricity consumption. The dominance of electricity-related impacts underscores the need to reduce energy consumption during the production process. This can be achieved by adopting energy-efficient equipment, optimizing manufacturing processes to reduce synthesis time, and exploring renewable or cleaner sources of electricity. **Figure 3.5.** illustrates the environmental impacts associated with PVDF membrane manufacturing. It presents a comprehensive breakdown of the individual chemical contributions

to various impact categories. Notably, regarding respiratory and smog effects, DMAc emerges as the predominant factor, while polyester plays a prominent role when considering ozone depletion impacts. When we delve into non-carcinogenic effects, global warming, eutrophication, ecotoxicity, carcinogenicity, and acidification, it becomes evident that electricity has the leading role in influencing these environmental impacts. This observation underscores the significance of electricity consumption during PVDF membrane production. In essence, DMAc and electricity consistently rank as the primary contributors across most impact categories. According to this study, there are several recommendations that can be offered to minimize the environmental impacts of PVDF membrane synthesis. To start with, it is advisable to contemplate the reduction of energy consumption in electrical equipment and the shortening of the synthesis time. Another suggestion is to explore alternative substitutes for DMAc to mitigate the environmental footprint associated with this manufacturing process.
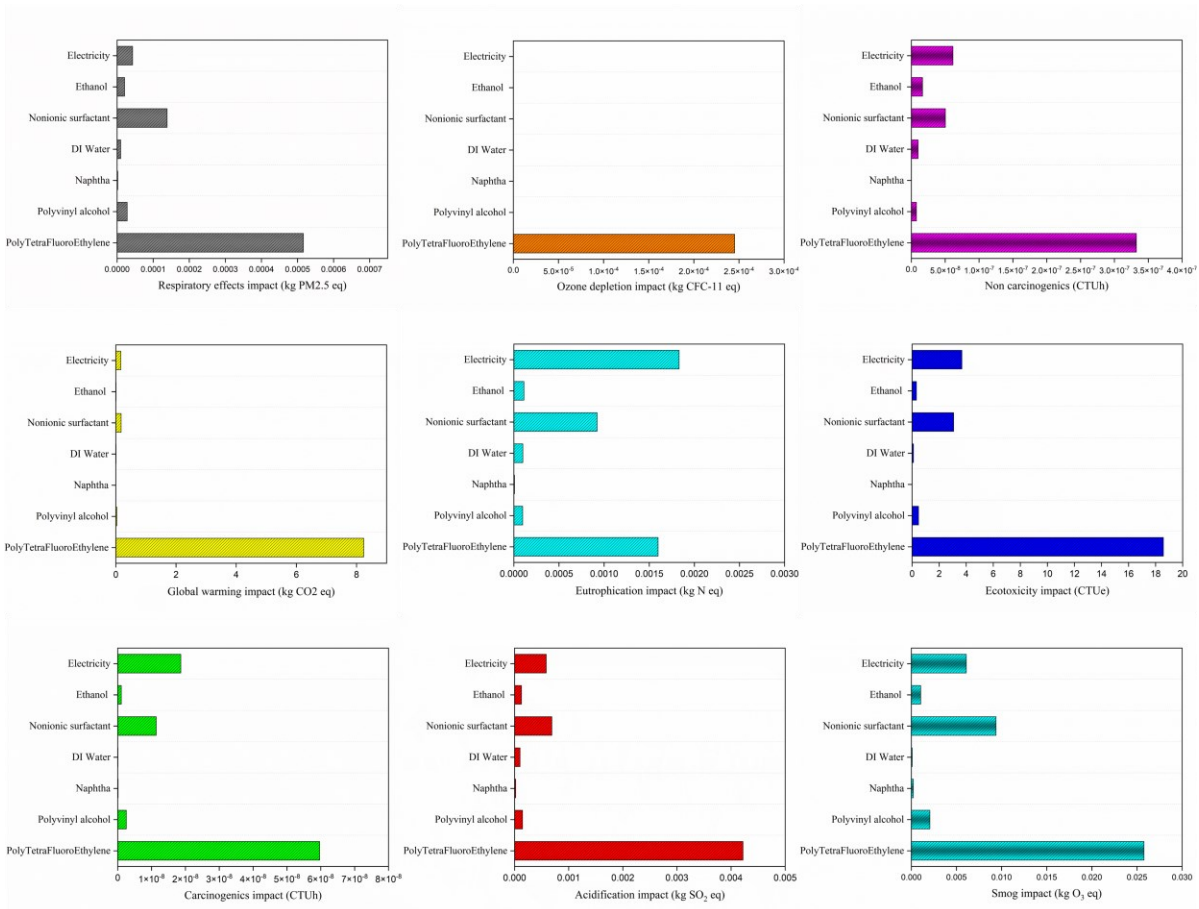
Figure 3.4. Contribution of each chemical to the environmental impacts of the synthesis of PTFE membrane.
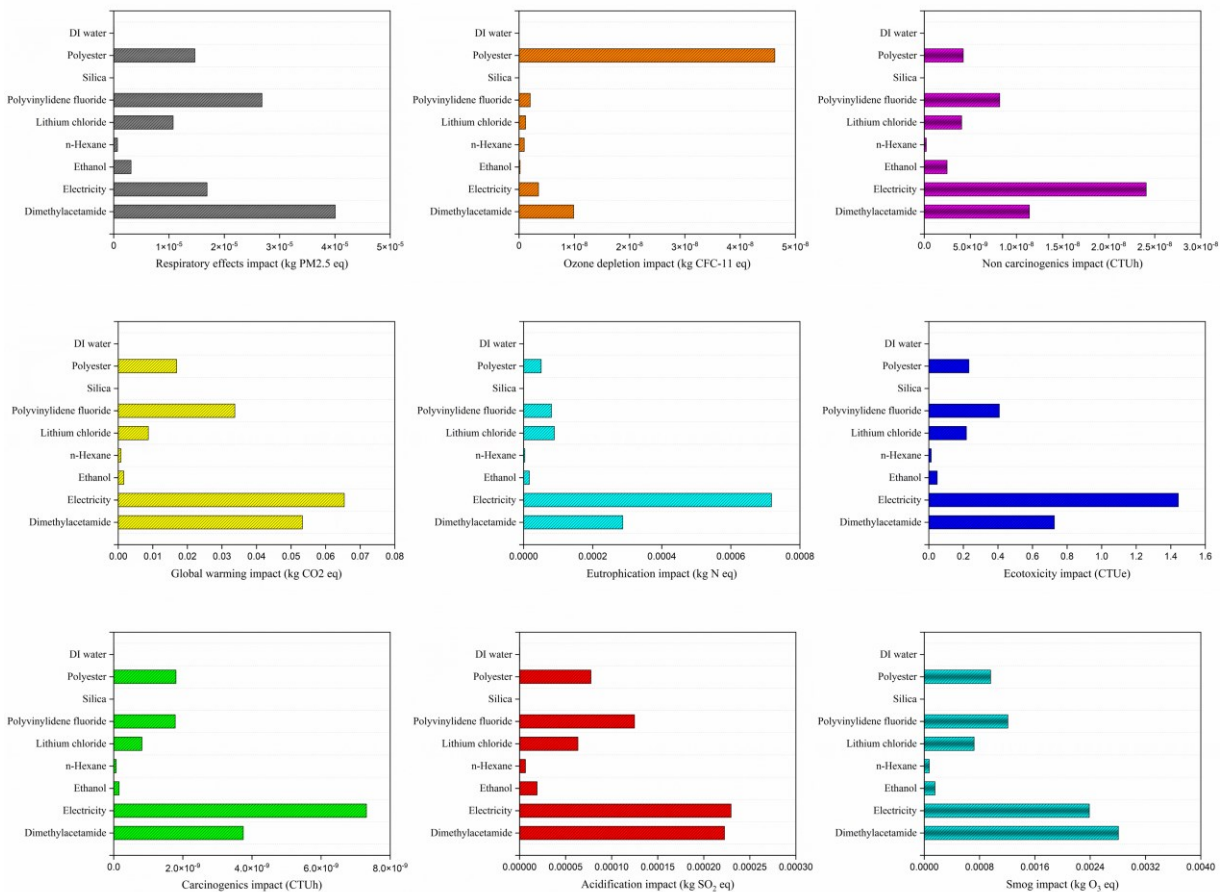
Figure 3.5. Contribution of each chemical to the environmental impacts of the synthesis of PVDF membrane.

3.3.2 Large-scale assessment

Moving on to the large-scale assessment, our focus was on generating power for 2000 people over a period of 10 days. Considering a daily power consumption of 25 kWh per person, we aimed to generate a total of 500,000 kWh of energy. To determine the membrane area required to achieve this energy generation goal using different types of membranes, we initially calculated the total energy production needed in watts (W) by dividing the watt-hours by the total number of hours in 10 days. After obtaining the total energy production needed in watts (W), we proceeded to find the required membrane area by dividing the total energy production (in W) by the power density (W/m²) of each membrane type. The power density values obtained from our modeling on the TOEC process were 2.986 W/m² for PVDF and 4.290 W/m² for PTFE membrane [114]. Based on our calculations, the required membrane area for generating large-scale power by the TOEC

process was found to be approximately 697,700.38 m² of PVDF membrane and 485,625.49 m² of PTFE membrane.

Figure 3.6.A presents a comparative analysis of PTFE and PVDF membranes concerning CED from various energy sources. The data reveals that, except for non-renewable sources, PVDF membranes exhibit a higher energy demand in all energy sources. Consequently, it can be concluded that for large-scale applications, PVDF membranes have higher energy demands than their PTFE counterparts. For large-scale applications, the higher energy demand of PVDF membranes can have significant implications. High energy demand not only impacts operational costs but also intensifies the carbon footprint and reliance on finite energy resources, particularly in cases where non-renewable sources are used. As industries continue to prioritize energy efficiency and environmental sustainability, the greater energy demand for PVDF membranes calls for careful consideration when choosing the appropriate membrane material for specific processes. In **Figure 3.6.B**, we delve into a comprehensive analysis of the two membranes across various environmental impact categories. The findings demonstrate that, apart from global warming and ozone depletion impact, PVDF membranes tend to exert a greater environmental footprint compared to PTFE membranes in most categories. The environmental implications of this comparative analysis highlight the importance of considering not only energy demand but also broader ecological factors when selecting membrane materials for specific applications. The choice of membrane material can significantly influence an operation's sustainability efforts and align with global initiatives to reduce greenhouse gas emissions and minimize ecological harm. In summary, the data suggests that, for large-scale applications of the TOEC process utilizing these membranes, PTFE membranes not only have less energy demand but are also more environmentally friendly than PVDF membranes. This information is instrumental in guiding decision-makers and industries toward more sustainable and energy-efficient choices, aligning with the imperative to mitigate environmental impacts in today's resource-conscious world.
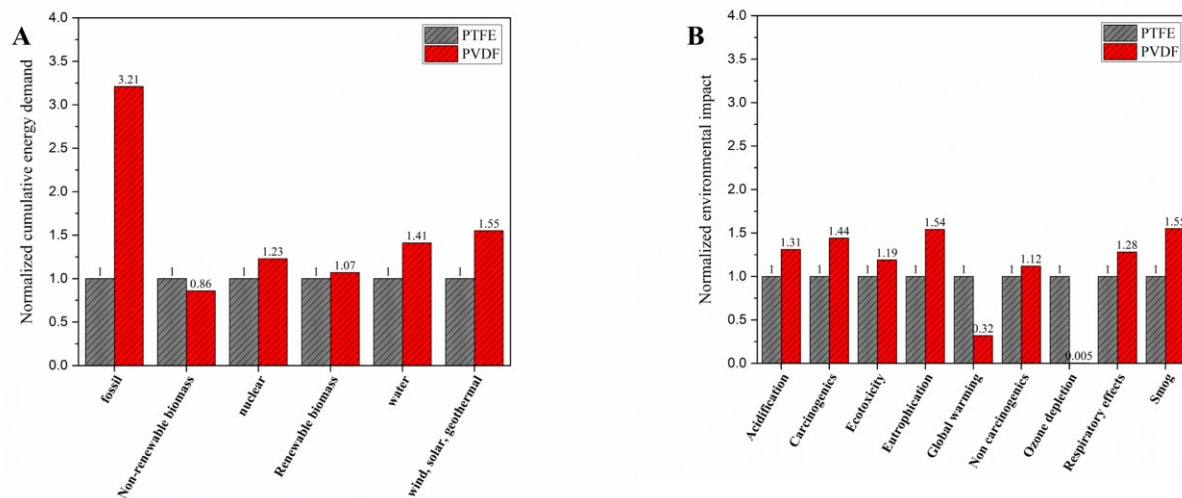
Figure 3.6. Large-scale evaluation of PTFE and PVDF membrane fabrication. (A) Comparative analysis of these membranes based on CED from various energy sources. (B) Comparative assessment of these membranes across multiple environmental impact categories.

3.4 Conclusion

In a world that demands energy efficiency, environmental responsibility, and sustainable energy solutions, the evaluation of membrane materials for the TOEC process is critical. The pioneering Life Cycle Assessment (LCA) conducted in this study sheds light on the environmental implications and cumulative energy demand (CED) of Polyvinylidene Fluoride (PVDF) and Polytetrafluoroethylene (PTFE) membranes throughout their entire life cycle, encompassing both laboratory-scale and large-scale production.

In the small-scale analysis, our findings highlighted the pivotal roles of fossil and renewable biomass sources as the primary contributors to the CED of both membranes. Furthermore, for PTFE membrane, the study demonstrated the varying degrees of chemical impact on the CED across different energy sources, with PTFE resin consistently emerging as a predominant contributor. Notably, PTFE resin, electricity, and nonionic surfactants played central roles in shaping the environmental footprint across various impact categories. On the other hand, the examination of PVDF membrane synthesis revealed the substantial impact of DMAc, electricity, and ethanol on its CED, with various chemicals assuming differing degrees of importance depending on the energy source. Environmental implications showcased that, for PVDF

membrane, DMAc and electricity consistently ranked as primary contributors across most environmental impact categories.

In the large-scale assessment, in order to compare both membranes, our research reveals that PVDF membranes exhibit higher energy demand across various energy sources, with the exception of non-renewable sources, compared to PTFE membranes. Furthermore, in most environmental impact categories, PVDF membranes tend to exert a more substantial environmental footprint. These results underscore the importance of considering not only energy demand but also broader environmental implications when choosing membrane materials for TOEC technology. The study's significance lies in its comprehensive coverage of both lab-scale synthesis and large-scale production of PTFE and PVDF membranes.

4   Conclusions and Future Work

4.1 Summary of Contributions and Results

In the context of escalating global energy demands and the imperative for sustainable energy solutions, exploring the Thermo-Osmotic Energy Conversion (TOEC) process has emerged as a potential avenue for tapping into low-grade waste heat and converting it into usable electricity. This conclusion chapter aims to combine and present the profound insights derived from the extensive examination of TOEC technology, the development of a robust model for simulating heat and mass transfer, and the enlightening life-cycle assessment of membrane synthesis for TOEC application.

The initial chapter delved into the background, challenges, and opportunities associated with TOEC technology, emphasizing the significance of harvesting low-grade waste heat to generate electricity. The analysis introduced the foundational principles of the TOEC process, laying the groundwork for subsequent in-depth exploration. The second chapter contributed a pioneering model for simulating heat and mass transfer within the TOEC process, introducing novelties such as the application of the ε-NTU method, consideration of membrane compaction, comprehensive examination of input variables, and conducting a systematic research of the process. The third chapter expanded the discussion by conducting a life-cycle assessment of membrane synthesis for TOEC, shedding light on the environmental implications and cumulative energy demand of polyvinylidene fluoride (PVDF) and polytetrafluoroethylene (PTFE) membranes.

The research efforts led to several pivotal findings. Developing a sophisticated TOEC model offered significant insights into the intricacies of heat and mass transfer within the process. By employing the ε-NTU method and thoroughly examining multiple input variables, the model provided avenues for potential systematic research in low-grade heat energy utilization. The modeling outcomes for the PTFE membrane with a pore size of 20 nm demonstrated that an optimal feed temperature of 65 ℃ is most favorable for attaining elevated TPC and vapor flow. Additionally, the analysis examined the influence of membrane properties, such as porosity and thickness. Increasing the membrane's porosity enhanced both TPC and the system's thermal

efficiency, while increasing membrane thickness produced the opposite effect. At a pressure of 9.4 bar, the utmost energy efficiency achievable with this membrane was 0.016%. A feed temperature surpassing 65 ∘C and a pressure on the cold side within the range of 6.2–11.8 bar are necessary to achieve a power density exceeding 5 W/m2 for the TOEC process. Our findings indicated that achieving high power density necessitates elevating the feed temperature and flow rates on both sides of the membrane, and reducing membrane thickness. The design map provided valuable direction to researchers, aiding in the adjustment of operational parameters and the utilization of ideal membrane characteristics. The findings from the model were highly consistent with both the experimental outcomes of this investigation and the existing literature.

Moreover, the life-cycle assessment of membrane synthesis significantly contributed to understanding the environmental impacts and cumulative energy demands of PTFE and PVDF membranes, offering critical insights into material selection for TOEC technology. The small-scale analysis identified the key contributors to cumulative energy demand and environmental impacts for both membranes, revealing the effects of various energy sources and chemical processes. The large-scale assessment facilitated a direct comparison, showing critical insights into the energy demands and environmental footprints of PTFE and PVDF membranes.

In conclusion, the extensive exploration and analyses presented in this thesis provide substantial contributions to the realm of sustainable energy generation. The insights derived from the TOEC model, coupled with the environmental perspectives gained from the life-cycle assessment, set forth a promising trajectory toward more efficient, environmentally responsible, and sustainable energy solutions.

4.2 Future Research Directions

Future research should focus on exploring and developing advanced membrane materials and technologies to enhance the efficiency and power density of the TOEC process. Investigating novel materials with superior properties, such as enhanced porosity, high LEP, stability, and selectivity, can significantly impact the overall performance of the system. Moreover, the exploration of innovative fabrication techniques or modifications in membrane structures may offer

improvements in terms of permeability, selectivity, and long-term stability, thereby advancing the TOEC process.

Integrating renewable energy sources within the TOEC process stands as a promising avenue for further research. Investigating the feasibility of coupling TOEC with renewable energy systems, such as solar or geothermal energy, could offer synergistic advantages, optimizing energy production and enhancing overall sustainability. Assessing the compatibility and potential synergies between TOEC and various renewable energy sources presents an exciting opportunity for future investigations. Furthermore, exploring configurations that involve multiple stages or hybrid designs could potentially boost energy conversion efficiency and power output. Investigating innovative system designs, such as cascading TOEC units or hybrid systems that combine TOEC with other energy conversion technologies, may unlock higher efficiencies and broader application potential.

Future studies should aim to scale up TOEC technology for commercial viability. It will be crucial to assess the feasibility of implementing TOEC systems at larger scales and optimizing their economic viability. This includes considering cost-effectiveness, scalability, and practical implementation in real-world industrial settings. Evaluating the technology's cost-benefit analysis, robustness, and adaptability to different industrial environments will be pivotal for its widespread adoption and commercialization.

Continued research efforts should focus on assessing and mitigating the environmental impact of TOEC systems. This entails conducting thorough life-cycle assessments to comprehend the technology's overall environmental footprint and implementing strategies to minimize its impact. Investigating environmentally friendly and sustainable practices in membrane synthesis is crucial, alongside ensuring proper disposal and recycling of materials involved in the process. These initiatives align with broader sustainability goals and emphasize environmental responsibility in advancing TOEC technology.

The exploration of these research avenues is anticipated to significantly contribute to advancing the understanding, efficiency, and practical application of TOEC technology, opening new horizons for sustainable and efficient energy conversion processes.

References

[1]   I. Gur, K. Sawyer, R. Prasher, Searching for a better thermal battery, Science (80-.). 335 (2012) 1454–1455.

[2]   T. Kim, M. Rahimi, B.E. Logan, C.A. Gorski, Harvesting energy from salinity differences using battery electrodes in a concentration flow cell, Environ. Sci. Technol. 50 (2016) 9791–9797.

[3]   C. Cheng, Y. Dai, J. Yu, C. Liu, S. Wang, S.P. Feng, M. Ni, Review of liquid-based systems to recover low-grade waste heat for electrical energy generation, Energy & Fuels. 35 (2020) 161–175.

[4]   M. Rahimi, A.P. Straub, F. Zhang, X. Zhu, M. Elimelech, C.A. Gorski, B.E. Logan, Emerging electrochemical and membrane-based systems to convert low-grade heat to electricity, Energy Environ. Sci. 11 (2018) 276–285.

[5]   D.B. Gingerich, M.S. Mauter, Quantity, quality, and availability of waste heat from United States thermal power generation, Environ. Sci. Technol. 49 (2015) 8297–8306.

[6]   I. Johnson, W.T. Choate, A. Davidson, Waste heat recovery. Technology and opportunities in US industry, BCS, Inc., Laurel, MD (United States), 2008.

[7]   S. Noamani, S. Niroomand, M. Rastgar, M. Azhdarzadeh, M. Sadrzadeh, Modeling of air-gap membrane distillation and comparative study with direct contact membrane distillation, Ind. Eng. Chem. Res. 59 (2020) 21930–21947.

[8]   S. Noamani, S. Niroomand, M. Rastgar, A. McDonald, M. Sadrzadeh, Development of a self-sustained model to predict the performance of direct contact membrane distillation, Sep. Purif. Technol. 263 (2021) 118407.

[9]   K. Park, D.Y. Kim, D.R. Yang, Theoretical analysis of pressure retarded membrane distillation (PRMD) process for simultaneous production of water and electricity, Ind. Eng. Chem. Res. 56 (2017) 14888–14901.

[10] A.P. Straub, M. Elimelech, Energy efficiency and performance limiting effects in thermo-osmotic energy conversion from low-grade heat, Environ. Sci. Technol. 51 (2017) 12925–12937.

[11] M. Rastgar, K. Moradi, C. Burroughs, A. Hemmati, E. Hoek, M. Sadrzadeh, Harvesting Blue Energy Based on Salinity and Temperature Gradient: Challenges, Solutions, and Opportunities, Chem. Rev. 123 (2023) 10156–10205.

[12] F. Mahmoudi, A. Date, A. Akbarzadeh, Further investigation of simultaneous fresh water production and power generation concept by permeate gap membrane distillation system, J. Memb. Sci. 572 (2019) 230–245.

[13] Y.M. Manawi, M.A.M.M. Khraisheh, A.K. Fard, F. Benyahia, S. Adham, A predictive model for the assessment of the temperature polarization effect in direct contact membrane distillation desalination of high salinity feed, Desalination. 341 (2014) 38–49.

[14] L. Martínez-Díez, M.I. Vazquez-Gonzalez, Temperature and concentration polarization in membrane distillation of aqueous salt solutions, J. Memb. Sci. 156 (1999) 265–273.

[15] A. Alkhudhiri, N. Darwish, N. Hilal, Membrane distillation: A comprehensive review, Desalination. 287 (2012) 2–18.

[16] M. Ciofalo, F. Ponzio, A. Tamburini, A. Cipollina, G. Micale, Unsteadiness and transition to turbulence in woven spacer filled channels for Membrane Distillation, in: J. Phys. Conf. Ser., IOP Publishing, 2017: p. 12003.

[17] M. Khayet, Membranes and theoretical modeling of membrane distillation: a review, Adv. Colloid Interface Sci. 164 (2011) 56–88.

[18] N.G.P. Chew, S. Zhao, R. Wang, Recent advances in membrane development for treating surfactant-and oil-containing feed streams via membrane distillation, Adv. Colloid Interface Sci. 273 (2019) 102022.

[19] K. Boussu, C. Kindts, C. Vandecasteele, B. Van der Bruggen, Surfactant fouling of nanofiltration membranes: measurements and mechanisms, ChemPhysChem. 8 (2007) 1836–1845.

[20] Z. Wang, S. Lin, Membrane fouling and wetting in membrane distillation and their mitigation by novel membranes with special wettability, Water Res. 112 (2017) 38–47.

[21] X. Yue, T. Zhang, D. Yang, F. Qiu, Z. Li, Y. Zhu, H. Yu, Oil removal from oily water by a low-cost and durable flexible membrane made of layered double hydroxide nanosheet on cellulose support, J. Clean. Prod. 180 (2018) 307–315.

[22] J. Israelachvili, R. Pashley, The hydrophobic interaction is long range, decaying exponentially with distance, Nature. 300 (1982) 341–342.

[23] A. Hausmann, P. Sanciolo, T. Vasiljevic, M. Weeks, K. Schroën, S. Gray, M. Duke, Fouling of dairy components on hydrophobic polytetrafluoroethylene (PTFE) membranes for membrane distillation, J. Memb. Sci. 442 (2013) 149–159.

[24] L.D. Tijing, Y.C. Woo, J.-S. Choi, S. Lee, S.-H. Kim, H.K. Shon, Fouling and its control in membrane distillation—A review, J. Memb. Sci. 475 (2015) 215–244.

[25] A.P. Straub, N.Y. Yip, S. Lin, J. Lee, M. Elimelech, Harvesting low-grade heat energy using thermo-osmotic vapour transport through nanoporous membranes, Nat. Energy. 1 (2016). https://doi.org/10.1038/nenergy.2016.90.

[26] S. Sinha Ray, H. Singh Bakshi, R. Dangayach, R. Singh, C.K. Deb, M. Ganesapillai, S.-S. Chen, M.K. Purkait, Recent developments in nanomaterials-modified membranes for improved membrane distillation performance, Membranes (Basel). 10 (2020) 140.

[27] G. Rácz, S. Kerker, O. Schmitz, B. Schnabel, Z. Kovacs, G. Vatai, M. Ebrahimi, P. Czermak, Experimental determination of liquid entry pressure (LEP) in vacuum membrane distillation for oily wastewaters, Membr. Water Treat. 6 (2015) 237–249.

[28] K.W. Lawson, D.R. Lloyd, Membrane distillation, J. Memb. Sci. 124 (1997) 1–25.

[29] E. Curcio, X. Ji, G. Di Profio, E. Fontananova, E. Drioli, Membrane distillation operated at high seawater concentration factors: Role of the membrane on $CaCO_3$ scaling in presence of humic acid, J. Memb. Sci. 346 (2010) 263–269.

[30] A.K. Kota, Y. Li, J.M. Mabry, A. Tuteja, Hierarchically structured superoleophobic surfaces with ultralow contact angle hysteresis, Adv. Mater. 24 (2012) 5838–5843.

[31] J. Ju, K. Fejjari, Y. Cheng, M. Liu, Z. Li, W. Kang, Y. Liao, Engineering hierarchically structured superhydrophobic PTFE/POSS nanofibrous membranes for membrane distillation, Desalination. 486 (2020) 114481.

[32] F. Zhao, Z. Ma, K. Xiao, C. Xiang, H. Wang, X. Huang, S. Liang, Hierarchically textured superhydrophobic polyvinylidene fluoride membrane fabricated via nanocasting for enhanced membrane distillation performance, Desalination. 443 (2018) 228–236.

[33] Y. Liao, R. Wang, A.G. Fane, Fabrication of bioinspired composite nanofiber membranes with robust superhydrophobicity for direct contact membrane distillation, Environ. Sci. Technol. 48 (2014) 6335–6341.

[34] D. Zhao, J. Zuo, K.-J. Lu, T.-S. Chung, Fluorographite modified PVDF membranes for seawater desalination via direct contact membrane distillation, Desalination. 413 (2017) 119–126.

[35] A.K. An, J. Guo, E.-J. Lee, S. Jeong, Y. Zhao, Z. Wang, T. Leiknes, PDMS/PVDF hybrid electrospun membrane with superhydrophobic property and drop impact dynamics for dyeing wastewater treatment using membrane distillation, J. Memb. Sci. 525 (2017) 57–67.

[36] K.-J. Lu, J. Zuo, T.-S. Chung, Tri-bore PVDF hollow fibers with a super-hydrophobic coating for membrane distillation, J. Memb. Sci. 514 (2016) 165–175.

[37] S. Pan, A.K. Kota, J.M. Mabry, A. Tuteja, Superomniphobic surfaces for effective chemical shielding, J. Am. Chem. Soc. 135 (2013) 578–581.

[38] H. Wang, H. Zhou, A. Gestos, J. Fang, H. Niu, J. Ding, T. Lin, Robust, electro-conductive, self-healing superamphiphobic fabric prepared by one-step vapour-phase polymerisation of poly (3, 4-ethylenedioxythiophene) in the presence of fluorinated decyl polyhedral oligomeric silsesquioxane and fluorinated alkyl silane, Soft Matter. 9 (2013) 277–282.

[39] Y. Sheen, Y. Huang, C. Liao, H. Chou, F. Chang, New approach to fabricate an extremely super-amphiphobic surface based on fluorinated silica nanoparticles, J. Polym. Sci. Part B Polym. Phys. 46 (2008) 1984–1990.

[40] A. Tuteja, W. Choi, J.M. Mabry, G.H. McKinley, R.E. Cohen, Robust omniphobic surfaces,

Proc. Natl. Acad. Sci. 105 (2008) 18200–18205.

[41]	M.R. Choudhury, N. Anwar, D. Jassby, M.S. Rahaman, Fouling and wetting in the membrane distillation driven wastewater reclamation process–A review, Adv. Colloid Interface Sci. 269 (2019) 370–399.

[42]	A.K. Kota, G. Kwon, A. Tuteja, The design and applications of superomniphobic surfaces, NPG Asia Mater. 6 (2014) e109–e109.

[43]	C. Boo, J. Lee, M. Elimelech, Engineering surface energy and nanostructure of microporous films for expanded membrane distillation applications, Environ. Sci. Technol. 50 (2016) 8112–8119.

[44]	R. Zheng, Y. Chen, J. Wang, J. Song, X.-M. Li, T. He, Preparation of omniphobic PVDF membrane with hierarchical structure for treating saline oily wastewater using direct contact membrane distillation, J. Memb. Sci. 555 (2018) 197–205.

[45]	S. Lin, S. Nejati, C. Boo, Y. Hu, C.O. Osuji, M. Elimelech, Omniphobic membrane for robust membrane distillation, Environ. Sci. Technol. Lett. 1 (2014) 443–447.

[46]	Z. Wang, D. Hou, S. Lin, Composite membrane with underwater-oleophobic surface for anti-oil-fouling membrane distillation, Environ. Sci. Technol. 50 (2016) 3866–3874.

[47]	D. Hou, C. Ding, K. Li, D. Lin, D. Wang, J. Wang, A novel dual-layer composite membrane with underwater-superoleophobic/hydrophobic asymmetric wettability for robust oil-fouling resistance in membrane distillation desalination, Desalination. 428 (2018) 240–249.

[48]	N.G.P. Chew, Y. Zhang, K. Goh, J.S. Ho, R. Xu, R. Wang, Hierarchically structured Janus membrane surfaces for enhanced membrane distillation performance, ACS Appl. Mater. Interfaces. 11 (2019) 25524–25534.

[49]	Y. Chen, K.-J. Lu, W. Gai, T.-S. Chung, Nanofiltration-inspired janus membranes with simultaneous wetting and fouling resistance for membrane distillation, Environ. Sci. Technol. 55 (2021) 7654–7664.

[50]	Y. Chen, K.-J. Lu, S. Japip, T.-S. Chung, Can composite Janus membranes with an ultrathin dense hydrophilic layer resist wetting in membrane distillation?, Environ. Sci. Technol. 54

(2020) 12713–12722.

[51] D. Feng, Y. Chen, Z. Wang, S. Lin, Janus membrane with a dense hydrophilic surface layer for robust fouling and wetting resistance in membrane distillation: new insights into wetting resistance, Environ. Sci. Technol. 55 (2021) 14156–14164.

[52] S.K. Hubadillah, Z.S. Tai, M.H.D. Othman, Z. Harun, M.R. Jamalludin, M.A. Rahman, J. Jaafar, A.F. Ismail, Hydrophobic ceramic membrane for membrane distillation: A mini review on preparation, characterization, and applications, Sep. Purif. Technol. 217 (2019) 71–84.

[53] Z.D. Hendren, J. Brant, M.R. Wiesner, Surface modification of nanostructured ceramic membranes for direct contact membrane distillation, J. Memb. Sci. 331 (2009) 1–10.

[54] A. Anvari, A.A. Yancheshme, K.M. Kekre, A. Ronen, State-of-the-art methods for overcoming temperature polarization in membrane distillation process: A review, J. Memb. Sci. 616 (2020) 118413.

[55] M.T. Rauter, S.K. Schnell, B. Hafskjold, S. Kjelstrup, Thermo-osmotic pressure and resistance to mass transport in a vapor-gap membrane, Phys. Chem. Chem. Phys. 23 (2021) 12988–13000.

[56] A. Razmjou, J. Mansouri, V. Chen, The effects of mechanical and chemical modification of TiO2 nanoparticles on the surface chemistry, structure and fouling performance of PES ultrafiltration membranes, J. Memb. Sci. 378 (2011) 73–84.

[57] C. Monteserín, M. Blanco, N. Murillo, A. Pérez-Márquez, J. Maudes, J. Gayoso, J.M. Laza, E. Hernáez, E. Aranzabe, J.L. Vilas, Novel antibacterial and toughened carbon-fibre/epoxy composites by the incorporation of TiO2 nanoparticles modified electrospun nanofibre veils, Polymers (Basel). 11 (2019) 1524.

[58] R.A. Damodar, S.-J. You, H.-H. Chou, Study the self cleaning, antibacterial and photocatalytic properties of TiO2 entrapped PVDF membranes, J. Hazard. Mater. 172 (2009) 1321–1328.

[59] A. Razmjou, E. Arifin, G. Dong, J. Mansouri, V. Chen, Superhydrophobic modification of

TiO2 nanocomposite PVDF membranes for applications in membrane distillation, J. Memb. Sci. 415 (2012) 850–863.

[60] K. Gethard, O. Sae-Khow, S. Mitra, Water desalination using carbon-nanotube-enhanced membrane distillation, ACS Appl. Mater. Interfaces. 3 (2011) 110–114.

[61] S. Leaper, A. Abdel-Karim, P. Gorgojo, The use of carbon nanomaterials in membrane distillation membranes: a review, Front. Chem. Sci. Eng. 15 (2021) 755–774.

[62] S.L. James, Metal-organic frameworks, Chem. Soc. Rev. 32 (2003) 276–288.

[63] J. Zuo, T.-S. Chung, Metal–organic framework-functionalized alumina membranes for vacuum membrane distillation, Water. 8 (2016) 586.

[64] K. Chen, L. Yao, F. Yan, S. Liu, R. Yang, B. Su, Thermo-osmotic energy conversion and storage by nanochannels, J. Mater. Chem. A. 7 (2019) 25258–25261.

[65] X. Zuo, C. Zhu, W. Xian, Q. Meng, Q. Guo, X. Zhu, S. Wang, Y. Wang, S. Ma, Q. Sun, Thermo-Osmotic Energy Conversion Enabled by Covalent-Organic-Framework Membranes with Record Output Power Density, Angew. Chemie Int. Ed. 61 (2022) e202116910.

[66] J. Li, Z. Zhang, R. Zhao, B. Zhang, Y. Liang, R. Long, W. Liu, Z. Liu, Stack thermo-osmotic system for low-grade thermal energy conversion, ACS Appl. Mater. Interfaces. 13 (2021) 21371–21378.

[67] M.S. Lee, J.W. Chang, K. Park, D.R. Yang, Energetic and exergetic analyses of a closed-loop pressure retarded membrane distillation (PRMD) for low-grade thermal energy utilization and freshwater production, Desalination. 534 (2022) 115799.

[68] X. Chen, C. Boo, N.Y. Yip, Low-temperature heat utilization with vapor pressure-driven osmosis: Impact of membrane properties on mass and heat transfer, J. Memb. Sci. 588 (2019) 117181.

[69] A.P. Straub, M. Elimelech, Energy Efficiency and Performance Limiting Effects in Thermo-Osmotic Energy Conversion from Low-Grade Heat, Environ. Sci. Technol. 51 (2017) 12925–12937. https://doi.org/10.1021/acs.est.7b02213.

[70] E. Shaulsky, V. Karanikola, A.P. Straub, A. Deshmukh, I. Zucker, M. Elimelech, Asymmetric membranes for membrane distillation and thermo-osmotic energy conversion, Desalination. 452 (2019) 141–148.

[71] T. Xiao, Z. Lin, C. Liu, L. Liu, Q. Li, Integration of desalination and energy conversion in a thermo-osmotic system using low-grade heat: Performance analysis and techno-economic evaluation, Appl. Therm. Eng. 223 (2023) 120039.

[72] M.Z. Hauschild, R.K. Rosenbaum, S.I. Olsen, Life cycle assessment, Springer, 2018.

[73] J.R. Barton, D. Dalley, V.S. Patel, Life cycle assessment for waste management, Waste Manag. 16 (1996) 35–50.

[74] M. Dadashi Firouzjaei, S.K. Nemani, M. Sadrzadeh, E.K. Wujcik, M. Elliott, B. Anasori, Life-Cycle Assessment of Ti3C2Tx MXene Synthesis, Adv. Mater. 35 (2023) 2300422.

[75] P. Miettinen, R.P. Hämäläinen, How to benefit from decision analysis in environmental life cycle assessment (LCA), Eur. J. Oper. Res. 102 (1997) 279–294.

[76] W. Lawler, J. Alvarez-Gaitan, G. Leslie, P. Le-Clech, Comparative life cycle assessment of end-of-life options for reverse osmosis membranes, Desalination. 357 (2015) 45–54.

[77] P.D. United Nations Department of Economic and Social Affairs, World population prospects 2022: Summary of results, (2022).

[78] D. Wang, X. Ling, H. Peng, L. Liu, L. Tao, Efficiency and optimal performance evaluation of organic Rankine cycle for low grade waste heat power generation, Energy. 50 (2013) 343–352.

[79] T.-C. Hung, T.Y. Shai, S.K. Wang, A review of organic Rankine cycles (ORCs) for the recovery of low-grade waste heat, Energy. 22 (1997) 661–667.

[80] H. Chen, D.Y. Goswami, E.K. Stefanakos, A review of thermodynamic cycles and working fluids for the conversion of low-grade heat, Renew. Sustain. Energy Rev. 14 (2010) 3059–3067.

[81] R.A. Kishore, D. Singh, R. Sriramdas, A.J. Garcia, M. Sanghadasa, S. Priya, Linear

thermomagnetic energy harvester for low-grade thermal energy harvesting, J. Appl. Phys. 127 (2020) 44501.

[82] L. Huang, A. He, M. Miao, J. Pei, T. Liu, X. Lei, K. Shan, S. Lei, Y. Wang, P. He, Simultaneous water and electricity harvesting from low-grade heat by coupling a membrane distiller and an electrokinetic power generator, J. Mater. Chem. A. 9 (2021) 27709–27717.

[83] S. Bai, C. Liu, Overview of energy harvesting and emission reduction technologies in hybrid electric vehicles, Renew. Sustain. Energy Rev. 147 (2021) 111188.

[84] X. Chen, M. Pan, X. Li, Novel supercritical CO2/organic Rankine cycle systems for solid-waste incineration energy harvesting: Thermo-environmental analysis, Int. J. Green Energy. 19 (2022) 786–807.

[85] I. Petsagkourakis, K. Tybrandt, X. Crispin, I. Ohkubo, N. Satoh, T. Mori, Thermoelectric materials and applications for energy harvesting power generation, Sci. Technol. Adv. Mater. 19 (2018) 836–862.

[86] W. Liu, X. Qian, C.-G. Han, Q. Li, G. Chen, Ionic thermoelectric materials for near ambient temperature energy harvesting, Appl. Phys. Lett. 118 (2021) 20501.

[87] C. Gao, S.W. Lee, Y. Yang, Thermally regenerative electrochemical cycle for low-grade heat harvesting, ACS Energy Lett. 2 (2017) 2326–2334.

[88] Q. Luo, A. He, S. Xu, M. Miao, T. Liu, B. Cao, K. Shan, B. Tang, X. Hu, L. Huang, Utilization of low-grade heat for desalination and electricity generation through thermal osmosis energy conversion process, Chem. Eng. J. 452 (2023) 139560.

[89] M. Rezaei, D.M. Warsinger, M.C. Duke, T. Matsuura, W.M. Samhaber, Wetting phenomena in membrane distillation: Mechanisms, reversal, and prevention, Water Res. 139 (2018) 329–352.

[90] S. Mosadegh-Sedghi, D. Rodrigue, J. Brisson, M.C. Iliuta, Wetting phenomenon in membrane contactors–causes and prevention, J. Memb. Sci. 452 (2014) 332–353.

[91] E. Guillen-Burrieza, A. Servi, B.S. Lalia, H.A. Arafat, Membrane structure and surface morphology impact on the wetting of MD membranes, J. Memb. Sci. 483 (2015) 94–103.

[92] P. Karami, B. Khorshidi, M. McGregor, J.T. Peichel, J.B.P. Soares, M. Sadrzadeh, Thermally stable thin film composite polymeric membranes for water treatment: A review, J. Clean. Prod. 250 (2020) 119447.

[93] P. Karami, B. Khorshidi, L. Shamaei, E. Beaulieu, J.B.P. Soares, M. Sadrzadeh, Nanodiamond-enabled thin-film nanocomposite polyamide membranes for high-temperature water treatment, ACS Appl. Mater. Interfaces. 12 (2020) 53274–53285.

[94] Z. Yuan, L. Wei, J.D. Afroze, K. Goh, Y. Chen, Y. Yu, Q. She, Y. Chen, Pressure-retarded membrane distillation for low-grade heat recovery: The critical roles of pressure-induced membrane deformation, J. Memb. Sci. 579 (2019) 90–101.

[95] J. Swaminathan, H.W. Chung, D.M. Warsinger, Membrane distillation model based on heat exchanger theory and configuration comparison, Appl. Energy. 184 (2016) 491–505.

[96] W.A. Phillip, Thermal-energy conversion: Under pressure, Nat. Energy. 1 (2016) 10–11. https://doi.org/10.1038/nenergy.2016.101.

[97] J.R. McCutcheon, M. Elimelech, Influence of membrane support layer hydrophobicity on water flux in osmotically driven membrane processes, J. Memb. Sci. 318 (2008) 458–466.

[98] S.S. Madaeni, S. Zinadini, V. Vatanpour, Preparation of superhydrophobic nanofiltration membrane by embedding multiwalled carbon nanotube and polydimethylsiloxane in pores of microfiltration membrane, Sep. Purif. Technol. 111 (2013) 98–107.

[99] K.G. Denbigh, Thermo-osmosis of gases through a membrane, Nature. 163 (1949) 60.

[100] V.M. Barragán, S. Kjelstrup, Thermo-osmosis in membrane systems: a review, J. Non-Equilibrium Thermodyn. 42 (2017) 217–236.

[101] D.R. Stull, Vapor pressure of pure substances. Organic and inorganic compounds, Ind. Eng. Chem. 39 (1947) 517–540.

[102] A.W. Adamson, A.P. Gast, Physical chemistry of surfaces, Interscience publishers New York, 1967.

[103] M. Khayet, M.K. Souhaimi, T. Matsuura, Membrane distillation: principles and

applications, (2011).

[104] M. Qtaishat, T. Matsuura, B. Kruczek, M. Khayet, Heat and mass transfer analysis in direct contact membrane distillation, Desalination. 219 (2008) 272–292.

[105] J. Phattaranawik, R. Jiraratananon, A.G. Fane, Effect of pore size distribution and air flux on mass transport in direct contact membrane distillation, J. Memb. Sci. 215 (2003) 75–85.

[106] A.R. Tehrani-Bagha, Waterproof breathable layers–A review, Adv. Colloid Interface Sci. 268 (2019) 114–135.

[107] K.M. Persson, V. Gekas, G. Trägårdh, Study of membrane compaction and its influence on ultrafiltration water permeability, J. Memb. Sci. 100 (1995) 155–162.

[108] M. del C. García-Payo, M.A. Izquierdo-Gil, C. Fernández-Pineda, Wetting study of hydrophobic membranes via liquid entry pressure measurements with aqueous alcohol solutions, J. Colloid Interface Sci. 230 (2000) 420–431.

[109] J. Phattaranawik, R. Jiraratananon, A.G. Fane, Heat transport and membrane distillation coefficients in direct contact membrane distillation, J. Memb. Sci. 212 (2003) 177–193.

[110] R.W. Schofield, A.G. Fane, C.J.D. Fell, Heat and mass transfer in membrane distillation, J. Memb. Sci. 33 (1987) 299–313.

[111] D.M. Van de Bor, C.A.I. Ferreira, A.A. Kiss, Low grade waste heat recovery using heat pumps and power cycles, Energy. 89 (2015) 864–873.

[112] B.K. Saha, B. Chakraborty, R. Dutta, Estimation of waste heat and its recovery potential from energy-intensive industries, Clean Technol. Environ. Policy. 22 (2020) 1795–1814.

[113] N. Jones, Waste heat: innovators turn to an overlooked renewable resource, Yale Environ. 360 (2018) 5.

[114] K. Moradi, M. Rastgar, P. Karami, A. Yousefi, S. Noamani, A. Hemmati, M. Sadrzadeh, Performance Analysis of the Thermo Osmotic Energy Conversion (TOEC) Process for Harvesting Low-Grade Heat, Chem. Eng. J. Adv. (2023) 100558.

[115] Q. Wu, A. Tiraferri, T. Li, W. Xie, H. Chang, Y. Bai, B. Liu, Superwettable PVDF/PVDF-

g-PEGMA ultrafiltration membranes, Acs Omega. 5 (2020) 23450–23459.

[116] S. Ashtiani, M. Khoshnamvand, P. Číhal, M. Dendisová, A. Randová, D. Bouša, A. Shaliutina-Kolešová, Z. Sofer, K. Friess, Fabrication of a PVDF membrane with tailored morphology and properties via exploring and computing its ternary phase diagram for wastewater treatment and gas separation applications, RSC Adv. 10 (2020) 40373–40383.

[117] X.-X. Ni, J.-H. Li, L.-P. Yu, A novel PVDF hybrid membrane with excellent active–passive integrated antifouling and antibacterial properties based on a PDA guiding effect, Mater. Adv. 2 (2021) 3300–3314.

[118] V. Shah, B. Wang, K. Li, High-performance PVDF membranes prepared by the combined crystallisation and diffusion (CCD) method using a dual-casting technique: a breakthrough for water treatment applications, Energy Environ. Sci. 14 (2021) 5491–5500.

[119] F. Zou, G. Li, X. Wang, A.L. Yarin, Dynamic hydrophobicity of superhydrophobic PTFE-SiO2 electrospun fibrous membranes, J. Memb. Sci. 619 (2021) 118810.

[120] Y. Tang, K. Sun, X. Du, J. Zhao, H. Wang, Q. Huang, Superhydrophobic electrospun FPI/PTFE nanofiber membranes for robust vacuum membrane distillation, Sep. Purif. Technol. 326 (2023) 124856.

[121] L.J. Müller, A. Kätelhön, M. Bachmann, A. Zimmermann, A. Sternberg, A. Bardow, A guideline for life cycle assessment of carbon capture and utilization, Front. Energy Res. 8 (2020) 15.

[122] X. Tian, S.D. Stranks, F. You, Life cycle energy use and environmental implications of high-performance perovskite tandem solar cells, Sci. Adv. 6 (2020) eabb0055.

[123] K. Hungerbühler, J.M. Boucher, C. Pereira, T. Roiss, M. Scheringer, K. Hungerbühler, J.M. Boucher, C. Pereira, T. Roiss, M. Scheringer, Life Cycle Assessment of Chemical Products and Processes, Chem. Prod. Process. Found. Environ. Oriented Des. (2021) 67–105.

[124] R. Frischknecht, F. Wyss, S. Büsser Knöpfel, T. Lützkendorf, M. Balouktsi, Cumulative energy demand in LCA: the energy harvested approach, Int. J. Life Cycle Assess. 20 (2015) 957–969.

[125] M.J.B. Kabeyi, O.A. Olanrewaju, Sustainable energy transition for renewable and low carbon grid electricity generation and supply, Front. Energy Res. 9 (2022) 1032.

[126] C.G. Solomon, R.N. Salas, D. Malina, C.A. Sacks, C.C. Hardin, E. Prewitt, T.H. Lee, E.J. Rubin, Fossil-fuel pollution and climate change—a new NEJM group series, N. Engl. J. Med. 386 (2022) 2328–2329.

[127] C. Manochio, B.R. Andrade, R.P. Rodriguez, B.S. Moraes, Ethanol from biomass: A comparative overview, Renew. Sustain. Energy Rev. 80 (2017) 743–755.

[128] S.C. McClelland, C. Arndt, D.R. Gordon, G. Thoma, Type and number of environmental impact categories used in livestock life cycle assessment: A systematic review, Livest. Sci. 209 (2018) 39–45.

[129] B.G. Hermann, C. Kroeze, W. Jawjit, Assessing environmental performance by combining life cycle assessment, multi-criteria analysis and environmental performance indicators, J. Clean. Prod. 15 (2007) 1787–1796.

[130] N.L. Pelletier, N.W. Ayer, P.H. Tyedmers, S.A. Kruse, A. Flysjo, G. Robillard, F. Ziegler, A.J. Scholz, U. Sonesson, Impact categories for life cycle assessment research of seafood production systems: review and prospectus, Int. J. Life Cycle Assess. 12 (2007) 414–421.

[131] M.M. Khasreen, P.F.G. Banfill, G.F. Menzies, Life-cycle assessment and the environmental impact of buildings: a review, Sustainability. 1 (2009) 674–701.